



Published in final edited form as:

*J Math Psychol.* 2018 December ; 87: 108–125. doi:10.1016/j.jmp.2018.10.001.

## Rotational-symmetry in a 3D scene and its 2D image

Tadamasa Sawada<sup>1</sup> and Qasim Zaidi<sup>2</sup>

<sup>1</sup>School of Psychology, National Research University Higher School of Economics

<sup>2</sup>SUNY Optometry - Graduate Center for Vision Research

### Abstract

A 3D shape of an object is  $N$ -fold rotational-symmetric if the shape is invariant for  $360/N$  degree rotations about an axis. Human observers are sensitive to the 2D rotational-symmetry of a retinal image, but they are less sensitive than they are to 2D mirror-symmetry, which involves invariance to reflection across an axis. Note that perception of the mirror-symmetry of a 2D image and a 3D shape has been well studied, where it has been shown that observers are sensitive to the mirror-symmetry of a 3D shape, and that 3D mirror-symmetry plays a critical role in the veridical perception of a 3D shape from its 2D image. On the other hand, the perception of rotational-symmetry, especially 3D rotational-symmetry, has received very little study. In this paper, we derive the geometrical properties of 2D and 3D rotational-symmetry and compare them to the geometrical properties of mirror-symmetry. Then, we discuss perceptual differences between mirror- and rotational symmetry based on this comparison. We found that rotational-symmetry has many geometrical properties that are similar to the geometrical properties of mirror-symmetry, but note that the 2D projection of a 3D rotational-symmetrical shape is more complex computationally than the 2D projection of a 3D mirror-symmetrical shape. This computational difficulty could make the human visual system less sensitive to the rotational-symmetry of a 3D shape than its mirror-symmetry.

### 1. Introduction

The human visual system is sensitive to the following three types of symmetry (Mach, 1906/1959): mirror (or bilateral or reflectional), rotational (or cyclic or radial)<sup>1</sup>, and translational (or repetition). Each type of symmetry is formally defined as an invariant against a particular transformation (Liu, Hel-Or, Kaplan, Van Gool, 2009; Weyl, 1952; Stewart & Golubitsky, 1992). For example, consider objects with rotational-symmetry. A 3D shape of a rotational-symmetrical object coincides with itself after rotating the object about its axis of symmetry for a particular angle (see Figure 1 for examples). Rotational-symmetry

---

**Publisher's Disclaimer:** This is a PDF file of an unedited manuscript that has been accepted for publication. As a service to our customers we are providing this early version of the manuscript. The manuscript will undergo copyediting, typesetting, and review of the resulting proof before it is published in its final citable form. Please note that during the production process errors may be discovered which could affect the content, and all legal disclaimers that apply to the journal pertain.

<sup>6</sup>It is possible to assert that this camera rotation transforms the vanishing point  $v_{axis}$  of the symmetry axis to the principal point so that the symmetry axis becomes normal to the image plane  $\Pi_I$  after the camera rotation.

<sup>1</sup>It is possible to assert that rotational-symmetry in Cartesian-coordinates is translational-symmetry in polar-coordinates (van der Helm & Leeuwenberg, 1996).

appears in many man-made objects, many flowers (Neal, Dafni, & Giurfa, 1998; Culbert & Forrest, 2016), some animal species (e.g. echinoderm and cnidarian), and local parts of plants and animals (Savriama & Klingenberg, 2011). It is also common in 2D image designs: e.g. texture patterns (Liu, Collins, Tsin, 2004; Clarke, Green, Halley, & Chantler, 2011; Westphal & Fitch, 2012) and logos (Hargittal & Hargittal, 1997).

Rotational-symmetry of a 2D image plays a role in visual perception and cognition, but its effects tend to be weaker than the effects of mirror-symmetry (see van der Helm & Leeuwenberg, 1996; Wagemans, 1995; Swaddle, 1999 for reviews). Rotational-symmetry can be reliably detected ( $d' > 1$ ) in a low-density random-dot pattern even with a brief viewing duration (100 ms) but it is not as easy to detect as mirror-symmetry (Figure 2a, b, Kahn & Foster, 1986; Wagemans, Van Gool, Swinnen, & Van Horebeek, 1993; see also Szlyk, Seiple, & Xie, 1995 for a relevant study). The detection of rotational-symmetry takes longer than the detection of mirror-symmetry (Royer, 1981; Palmer & Hemenway, 1978). Julesz (1971) showed that rotational-symmetry is hard to detect in a high-density random-dot pattern while mirror-symmetry is easily detected (Figure 2c, d). Past studies have shown that figures with rotational-symmetry are rated as “good” (Palmer, 1991; Garner & Clement, 1963), rated as “organized” (Hershenson & Ryder, 1982, see also Wagemans, 1997), and associated with positive words (Makin, Pecchinenda, & Bertamini, 2012) more often than asymmetrical figures are, but less often than mirror-symmetrical figures are (see also Hamada & Ishihara, 1988; Hamada et al., 2016 for inconsistent results).

Results of brain imaging studies suggest that the ventral stream in the visual system is involved in processing 2D rotational-symmetry. Both rotational- and mirror-symmetry induce sustained posterior negativity of the ERP signal measured from two occipital electrodes (PO7 and PO8 according to the international 10–20 system) 300ms after the onset of the stimuli (Makin, Wilton, Pecchinenda, & Bertamini, 2012; Makin, Rampone, Pecchinenda, & Bertamini, 2013). This induced effect is stronger for mirror-symmetry than for rotational-symmetry. Based on a source localization analysis of the ERP signal, the effect is caused primarily by activity in the lateralized extrastriate visual cortex (Makin, Wilton et al., 2012). Kohler, Clarke, Yakovleva, Liu, and Norcia (2016) showed that rotational-symmetry in a texture pattern is parametrically represented in V3 and in later visual areas in the ventral stream (V4, VO1, and LOC) using fMRI and EEG.

The 3D rotational-symmetry of an object can play some role in the perception of the object’s 3D shape. The perception of the center-of-gravity of an object becomes more accurate if the object is rotational-symmetrical (Bingham & Muchisky, 1993a, b). According to Biederman’s Recognition-by-components theory, a complex 3D shape of an object can be decomposed into simpler parts called “geons” (Biederman, 1987; see also Pentland, 1986; Binford, 1971 for analogous ideas). Some of the geons used in past studies (Biederman & Gerhardstein, 1993) were 3D rotational-symmetrical. Note that the perception of 3D rotational-symmetry has been studied much less often than 3D mirror-symmetry.

Now, consider human’s visual perception of mirror-symmetry. Humans can detect the mirror-symmetry of a retinal image efficiently (e.g. Barlow & Reeves, 1979; Jenkins, 1983; Cohen & Zaidi, 2013), of a non-frontoparallel planar figure (Sawada & Pizlo, 2008;

Wagemans, 1992, 1993; van der Vloed, Csathó, & van der Helm, 2005; Szlyk, Rock, & Fisher, 1995), and of a volumetric object (Sawada, 2010). Moreover, mirror-symmetry also plays a critical role in the perception of the shapes of planar figures (Sawada, 2008; Saunders & Knill, 2001) and of volumetric objects (Pizlo, 2008; Li, Pizlo, & Steinman, 2009; Li, Sawada, Shi, Kwon, & Pizlo, 2011; Pizlo, Sawada, Li, Kropatsch, & Steinman, 2010; Pizlo, Li, Sawada, & Steinman, 2014). Mirror-symmetry of the volumetric object allows us to recover a complete 3D shape of the object including its invisible back part from a single 2D image of the object (Mitsumoto, Tamura, Okazaki, Kajimi, & Fukui, 1992; Pizlo et al., 2010, 2014; Michaux, Kumar, Jayadevan, Delp, & Pizlo, 2017). It is important to recover the complete 3D shape of the object for interacting with the object (Varley, DeChant, Richardson, Ruales, & Allen, 2017).

The high sensitivity of human's to mirror-symmetry is often explained teleologically. For example, many objects around us are mirror-symmetrical and mirror-symmetry serves as an important factor for sexual selection of many animals (Møller & Thornhill 1998; Møller, Thornhill, & Gangestad, 2005). Furthermore, the mirror-symmetry of an object introduces unique geometrical properties into its 3D shape and into its 2D retinal image (e.g. Vetter & Poggio, 1994; Sawada, 2010; Sawada, Li, & Pizlo, 2014). These geometrical properties can play an important role in the perception of mirror-symmetry (Sawada, Li, & Pizlo, 2015; Pizlo et al., 2014).

In this study, we derive the geometrical properties of 2D and 3D rotational-symmetry that correspond to geometrical properties of mirror-symmetry and then compare these properties between the two types of symmetry. This comparison allows us to analytically discuss human perception and cognition of rotational- and mirror-symmetry.

## 2. Definition

In this study, it is assumed that all 2D and 3D curves are “tame”: (i) they are finitely long and are decomposed into a finite number of segments that are also finitely long, (ii) are continuously twice differentiable, (iii) each segment of the 2D curve does not have any intersection with a tangent line at every non-endpoint of the segment (see Latecki & Rosenfeld, 1998 for a further discussion), (iv) each segment of the 3D curve does not intersect with a rectifying plane at every non-endpoint of the segment (A. Michaux, personal communication, May 8, 2013). The rectifying plane is tangent to the segment and is perpendicular to a plane of curvature at the point (Hilbert & Cohn-Vossen, 1952). The  $XYZ$  Cartesian coordinate system of a 3D scene and the  $xy$  Cartesian coordinate system of a 2D image in the scene are set as follows: (i) the  $Z$ -axis of the 3D coordinate system is perpendicular to the image plane  $\Pi_I$  and  $\Pi_I$  is  $Z = f$  where  $f$  is a constant, (ii) the  $Z$ -axis passes through the origin of the 2D coordinate system, and (iii) the  $X$ - and  $Y$ -axes of the 3D coordinate system are parallel to the  $x$ - and  $y$ -axes of the 2D coordinate system, respectively. Under an orthographic projection, a 2D orthographic projection  $[x_{o2D} y_{o2D}]^T$  of a point  $[X_{3D} Y_{3D} Z_{3D}]^T$  in a 3D scene is:

$$[x_{o2D} \ y_{o2D}]^T = [X_{3D} \ Y_{3D}]^T$$

Under a perspective projection, the origin of the 3D coordinate system is at a “center of projection”  $F$ . Note that the  $Z$ -axis passes  $F$ , intersects with the image plane  $\Pi_f$  at the origin of the 2D coordinate system on  $\Pi_f$ , and is normal to  $\Pi_f$ . Then, the  $Z$ -axis is referred as the principal axis and the intersection is referred as the principal point of the perspective projection. If  $f$  is the focal distance of the camera, a 2D perspective projection of  $[X_{3D} \ Y_{3D} \ Z_{3D}]^T$  is  $[x_{p2D} \ y_{p2D}]^T = [fX_{3D}/Z_{3D} \ fY_{3D}/Z_{3D}]^T$  and this relation can be written as:

$$\begin{bmatrix} x_{p2D}^* \\ y_{p2D}^* \\ w_{p2D}^* \end{bmatrix} = \begin{pmatrix} f & 0 & 0 \\ 0 & f & 0 \\ 0 & 0 & 1 \end{pmatrix} \begin{bmatrix} X_{3D} \\ Y_{3D} \\ Z_{3D} \end{bmatrix}$$

where  $[x_{p2D}^* \ y_{p2D}^* \ w_{p2D}^*]^T$  is called the homogeneous coordinates of  $[x_{p2D} \ y_{p2D}]^T$  and  $[x_{p2D} \ y_{p2D}]^T = [x_{p2D}^*/w_{p2D}^* \ y_{p2D}^*/w_{p2D}^*]^T$ .

A 2D rotation can be written as:

$$R_{2D}(\sigma_{2D}) = \begin{pmatrix} \cos\sigma_{2D} & -\sin\sigma_{2D} \\ \sin\sigma_{2D} & \cos\sigma_{2D} \end{pmatrix}$$

where  $\sigma_{2D}$  is an angle of the rotations. Note that the 3D  $XYZ$  Cartesian coordinate system used in this study is right-handed. Hence, rotations  $R_X$ ,  $R_Y$ , and  $R_Z$  around the  $X$ -,  $Y$ -, and  $Z$ -axes can be represented by the following rotation matrices:

$$R_X(\sigma_X) = \begin{pmatrix} 1 & 0 & 0 \\ 0 & \cos\sigma_X & -\sin\sigma_X \\ 0 & \sin\sigma_X & \cos\sigma_X \end{pmatrix},$$

$$R_Y(\sigma_Y) = \begin{pmatrix} \cos\sigma_Y & 0 & \sin\sigma_Y \\ 0 & 1 & 0 \\ -\sin\sigma_Y & 0 & \cos\sigma_Y \end{pmatrix},$$

$$R_Z(\sigma_Z) = \begin{pmatrix} \cos\sigma_Z & -\sin\sigma_Z & 0 \\ \sin\sigma_Z & \cos\sigma_Z & 0 \\ 0 & 0 & 1 \end{pmatrix}$$

where  $\sigma_X$ ,  $\sigma_Y$ , and  $\sigma_Z$  are angles of the rotations.

### 3. Theorems and Proofs

#### 3.1. 2D rotational-symmetry

Rotational-symmetry can be characterized by its degree of “fold”<sup>2</sup>. Consider a 2D  $n$ -fold symmetrical shape where  $n \geq 2$  (Figure 3). This shape is invariant against its rotation around its symmetry point for  $360/i$  degree where  $i$  is an integer. The symmetry point is at the center of gravity (CoG) of the shape. A set of  $n$  points of the shape are symmetrically corresponded if a position of their  $j$ -th point after a rotation for  $360/i$  degree coincide with a position of their  $((j + i) \% n)$ -th point before the rotation where  $j$  is an integer and  $\%$  represents the modulo operation. For a planar symmetrical figure in a 3D scene, its symmetry axis is defined as a line that is normal to the plane of the figure and that passes the symmetry point. If  $n = 2$ , the rotation angle of symmetry is 180 degrees and each pair of points symmetrically corresponded in the shape can be connected by a line-segment whose midpoint is at the symmetry point. If  $n > 2$ ,  $n$  corresponding points form a regular  $n$ -sided polygon whose CoG appears at the symmetry point. Now let us call these “regular polygons” and the line-segments connecting the corresponding points “symmetry polygons”. If  $n = 2$ , the symmetry polygon is a line-segment that is an “open polygon.” The symmetry polygons of 2-fold symmetry are also called symmetry line-segments in this study. When  $n \rightarrow \infty$ , the symmetry polygon becomes a circle, which is the most regular shape (Pizlo, 2008, see also Metzger, 1936/2009).

**3.1.1. Skewed rotational-symmetry**—Consider a planar  $n$ -fold symmetrical figure slanted relative to the observer. The image produced by slanting a planar figure is called *skewed symmetry* (Kanade, 1981; Kanade & Kender, 1983). Some properties of the symmetry of the figure are preserved in skewed symmetry under both orthographic and perspective projections as model-based invariants (Sawada, Li, & Pizlo, 2015; Rothwell, 1995). The human visual system detects mirror-symmetry of a planar figure and of a volumetric object based on an invariant of mirror-symmetry under an orthographic projection (Sawada & Pizlo, 2008; Sawada, 2010; Wagemans, 1995). It is possible that some invariant of rotational-symmetry could be also important for the visual system to detect rotational-symmetry. We discuss model-based invariants of rotational-symmetry under the projections.

Now, consider an orthographic projection of a planar symmetrical figure to a 2D image plane. The orthographic projection is a 2D compression along the orientation of a slant  $\sigma_{slant}$  of the planar figure by a factor of  $\cos(\sigma_{slant})$ . The 3D orientation of the figure can be computed from the compression of the projection of the symmetry polygon if the number of the symmetry folds of the figure is more than 2. A symmetry point of the figure is projected to the CoG of the image of the figure. Note that if the number of the symmetry folds of the figure is even, the orthographic projection is also 2-fold symmetrical (see images of 2- and 4-fold symmetrical figures in Figure 4).

<sup>2</sup>From here on, we will use “symmetry” to mean “rotational-symmetry” unless something else is specified.

Under a perspective projection, the 3D orientation of the figure can be computed from its single symmetry polygon if the number of folds  $n$  of the figure is more than 3 (see also Van Gool, Moons, & Proesmans, 1996). The symmetry polygon is an  $n$ -sided regular polygon and mirror symmetrical with  $n$  symmetry axes. This mirror-symmetry of the symmetry polygon can be used to compute the 3D orientation of the polygon (Hong, Yang, Huang, & Ma, 2004; Yang, Huang, Rao, Hong, & Ma, 2005). Note that the symmetry point is not projected to the CoG of the image of the figure under the perspective projection. The projection of the symmetry point coincides with a projection of the CoG of a symmetry polygon of the figure. A projection of the CoG can be derived from the fact that every symmetry polygon is a regular polygon. Now consider the following four cases for finding a projection of the CoG of a symmetry polygon that depend on the number of folds  $n$  of the figure, namely, i)  $n > 3$  and  $n$  is even, ii)  $n > 3$  and  $n$  is odd, iii)  $n = 3$ , and iv)  $n = 2$ . First, consider the case in which  $n > 3$  and  $n$  is even. Each symmetry polygon of the figure is a regular  $n$ -sided polygon. The CoG of the symmetry polygon can be determined by drawing auxiliary line-segments each of which connects the pair of a vertex of the symmetry polygon with the next vertex but  $(n - 2)/2$  (see Figure 5A for  $n = 4$ ). Specifically, the  $i$ -th vertex of a  $n$ -fold symmetry polygon is connected with  $(i + (n - 2)/2)$ -th vertex. These line-segments intersect with one another at the CoG of the symmetry polygon. A projection of the intersection of the line-segments is an intersection of the line-segments that are projections of these line-segments. It follows that the projection of the CoG can be derived by finding an intersection of the line-segments that connect the vertices of the projection of the symmetry polygon (Figure 5C).

If  $n > 3$  and  $n$  is odd, the CoG of the symmetry polygon and its projection can be determined in an analogous way. The CoG of the symmetry polygon is an intersection of line-segments, each of which connects a vertex of the symmetry polygon with a midpoint of an edge between the next vertices of the symmetry polygon but  $(n-1)/2$  and  $(n-3)/2$ . Note that the midpoint of the edge, however, is not projected to a midpoint of a projection of the edge under a perspective projection. On the other hand, an intersection of two lines is projected to an intersection of projections of the lines under both the perspective and orthographic projections. Here, instead of using the midpoints, the line-segments that pass the CoG of the symmetry polygon can be drawn by drawing additional auxiliary line-segments and using their intersections (see a case  $n = 5$  in Figure 5A). Each of these additional auxiliary line-segments connects a vertex of the symmetry polygon with the vertex after the next vertex. Namely, the  $i$ -th vertex of a  $n$ -fold symmetry polygon is connected with the  $(i \pm 2)$ -th vertex. With this in place, an  $n$ -pointed star appears within the symmetry polygon. Note that the symmetry polygon is a regular  $n$ -sided polygon and is 2D mirror-symmetrical with  $n$ -symmetry axes. The star is also 2D mirror-symmetrical about the symmetry axes of the symmetry polygon because the auxiliary line-segments connects vertices of the symmetry polygon in a symmetrical manner (the  $i$ -th vertex of the symmetry polygon is connected with the  $(i \pm 2)$ -th vertex). Each symmetry axis connects the  $i$ -th vertex of the star with the  $(i+n)$ -th vertex of the star. The symmetry axes intersect at the CoG of the star, which is at the CoG of the symmetry polygon. It is because a symmetry axis of any 2D mirror-symmetrical polygon passes the CoG of this polygon. Recall that an intersection of two lines is projected to an intersection of projections of the lines under both the perspective and orthographic

projections. The projection of the CoG can be derived by drawing auxiliary line-segments in the same way in the projection of the symmetry polygon (see cases  $n = 5$  in Figure 5B and C). These methods using the auxiliary line-segments for finding the image of the center of gravity for  $n > 3$  can also be applied to an orthographic projection.

If  $n = 3$ , the projection of the CoG of the individual symmetry polygon cannot be determined uniquely. Now, assume that the center of the perspective projection from the symmetrical figure to the 2D image is given (calibrated camera, see Li, Sawada, Latecki, Steinman, & Pizlo, 2012). The shape of the 3D symmetry polygon is also known (a regular triangle), and that its 2D projection is a triangle, except when it is presented in a degenerate view. It is often impossible to determine, uniquely, the 3D orientation of a symmetry polygon from a 2D triangle of its projection (Fischler & Bolles, 1981; Gao, Hou, Thang, & Cheng, 2003; Minkov & Sawada, 2018). There can be up to four possible 3D orientations of a symmetry polygon for its 2D triangle and, when there are, its CoG is projected to different positions within the 2D image, depending on the symmetry polygon's orientation (see Figure 6). If the planar figure has multiple symmetry polygons, their CoGs must coincide with one another and a unique CoG can be determined. Then, the 3D orientation of the figure can be uniquely determined.

If  $n = 2$ , the symmetry polygon is a line-segment (symmetry line-segment) and its symmetry point is at the midpoint of the line-segment. The perspective projection of the midpoint, however, is not a midpoint of the perspective projection of the symmetry line-segment. If a planar figure with 2-fold symmetry has multiple symmetry line-segments, these line-segments intersect with one another at their midpoints. Otherwise, a vanishing point  $v_i^3$  of the symmetry line-segment is required to derive a perspective projection  $m_i$  of its midpoint  $M_i$ . Note that  $v_i$  and  $m_i$  are collinear with the projection of the line-segment and their relationship can be written as (see supplemental material):

$$r_{mi} = \frac{2r_{\phi i}r_{\psi i}}{r_{\phi i} + r_{\psi i}} \quad (1)$$

where  $r_{mi}$ ,  $r_{\phi i}$ , and  $r_{\psi i}$  are distances from  $v_i$  to  $m_i$  and two endpoints of the projection of the line-segment. If the planar figure has multiple symmetry line-segments, they intersect at their common CoG. Then, their vanishing points can be computed from Equation (1) and the 3D orientation of the figure can be uniquely determined.

### 3.2. 3D rotational-symmetry

A 3D symmetrical object has a symmetry axis that is normal to the symmetry polygons of the 3D object and passes their CoGs (Figure 7). When  $n \rightarrow \infty$ , the symmetry polygon becomes a circle and the whole symmetrical object becomes a surface-of-revolution (SoR).

<sup>3</sup>Consider a perspective projection of a line segment in a 3D scene to an image plane. The vanishing point of the segment can be uniquely determined so that the vanishing point and the center of projection can be connected by a line that is parallel to the segment. Any line parallel to the segment is projected to a pair of collinear half-lines that emanate from the vanishing point unless the line passes the center of projection.

Note that a single 3D object can have multiple symmetry axes. For example, a cube has three axes for a 4-fold symmetry, four axes for a 3-fold symmetry, and six axes for a 2-fold symmetry.

A 2D image of a 3D  $n$ -fold symmetrical object becomes 2D  $n$ -fold symmetrical only from an accidental view-point. The image is  $n$ -fold symmetrical when the symmetry axis is normal to a plane of the image under an orthographic projection and when the symmetry axis coincides with the principal axis under a perspective projection<sup>4</sup>. If it does not,  $n$ -fold symmetry is not present in the image.

### 3.2.1. A 3D symmetrical object and its 2D image

**3.2.1.1. Properties of a 2D image of a 3D symmetrical object:** A 3D symmetrical object has multiple symmetry polygons whose CoGs are collinear along its symmetry axis. This collinearity is a model-based invariant under both orthographic and perspective projections. Projections of the CoGs are also collinear with a projection of the symmetry axis in a 2D image of the symmetrical object. It follows that the projection of the symmetry axis can be derived if the projections of the CoGs of the multiple symmetry polygons can be detected in the image (see 3.1.1.). Detecting the symmetry axis from the image allows the visual system to see symmetry of the whole object rather than symmetry of its individual symmetry polygons. The individual symmetry polygons are formed by local features of the object and the whole object is composed of the local features so that their symmetry polygons share the common symmetry axis. If there is no common symmetry axis among the symmetry polygons, the whole object cannot be symmetrical but can have some symmetrical parts.

Consider a perspective projection of the 3D symmetrical object to an image plane. The vanishing point of the symmetry axis in the image plane can be determined so that a line connecting the vanishing point and the center of projection is parallel to the symmetry axis. The symmetry polygons of the 3D object are planar and perpendicular to the symmetry axis. It follows that if  $n > 2$ , the symmetry polygons are parallel to one another and their horizons coincide with a single line in the 2D image. A plane connecting the horizon and the center of projection is parallel to the symmetry polygons (see 3.1.1.) and this plane is perpendicular to the line connecting the vanishing point and the center of projection (Figure 8).

The vanishing point of the symmetry axis and the horizon of the symmetry polygons can be determined from the 2D perspective image of the 3D symmetrical object. If  $n > 3$ , each symmetry polygon and its auxiliary lines always form two or more than two sets of parallel line segments. The parallel line segments in each set are projected to line segments converging at their vanishing point that is on the horizon of the symmetry polygon. Hence, the horizon can be determined as a line passing the vanishing points of the sets of parallel line segments. If  $n = 3$ , a symmetry polygon is a regular triangle and its 3D orientation cannot be always determined uniquely from the projection of the symmetry polygon. The projection is consistent with up to four 3D orientations of the symmetry polygon. The

---

<sup>4</sup>With a reduced eye, whose center of projection is at a center of its spherical retina, the retinal image of a 3D  $n$ -fold symmetrical object is 2D  $n$ -fold symmetrical if the symmetry axis passes through the center of projection.

orientation can be uniquely determined if there is another symmetry polygon. Their orientations are determined so that they are parallel to one another in a 3D scene.

If  $n = 2$ , the symmetry polygons are line-segments (symmetry line-segments). Their vanishing points appear on a horizon of a plane that is perpendicular to the symmetry axis. The symmetry line-segments are perpendicular to a normal to a plane connecting the horizon and the center of projection. A perspective projection of a symmetry line-segment alone is not enough to determine the projection of its CoG. Determining this requires having a vanishing point of the symmetry line-segment. Vanishing points of symmetry line-segments of a single 3D symmetrical object can be derived if the number of the symmetry line-segments is three, or more than three (see also 3.1.1.). In the 2D perspective image of the 3D object, vanishing points of the symmetry line segments are collinear on a line (Figure 9). This line is the horizon of a plane to which the symmetry line-segments are parallel and the symmetry axis is normal. The plane is normal to a line connecting the vanishing point of the symmetry axis and the center of projection. The vanishing point of the symmetry axis can be found by using an optimization process. The space for this optimization process is two dimensional, specifically the 2D position of the vanishing point of the symmetry axis in the image. For a given position of the vanishing point, projections of the midpoints of the symmetry line-segments can be derived. Note that the midpoints of the symmetry line-segments are collinear on the symmetry axis and their projections are also collinear. Then, validity of the given position can be evaluated based on the collinearity of the projections of the midpoints. The projections of the midpoints are derived in the following steps. First, the horizon of the symmetry line-segments is determined from the given position of the vanishing point of the symmetry axis. Then, the vanishing points of the symmetry line-segments are found at intersections of the horizon with lines of the projections of the symmetry line-segments. From the vanishing points of the symmetry line-segments, the projections of their midpoints can be derived (Equation 1).

### 3.2.2. Recovering a 3D rotational-symmetrical shape from a single 2D image

—The 3D shape of a 3D mirror-symmetrical object can be recovered from its single 2D image uniquely under a perspective projection (Gordon, 1990; Rothwell, 1995; Hong, Yang, Huang, & Ma, 2004; Yang, Huang, Rao, Hong, & Ma, 2005) and up to a one unknown parameter under an orthographic projection (Vetter & Poggio, 1994). This geometrical property has been used for modeling veridical perception of the 3D shape of the mirror-symmetrical object (Pizlo, 2008; Pizlo et al., 2010, 2014).

The 3D shape of a 3D rotational-symmetrical object can also be recovered from its single 2D image by using two different methods. The first method is based on Multiple-view geometry (Hartley & Zisserman, 2004). It uses a “virtual image” of the 3D symmetrical object (Vetter & Poggio, 1994). Note that the shape of the object is invariant against a rotation  $R_{axis}$  around the symmetry axis of the object for  $360i/n$  degree, where  $n$  is the number of symmetry folds of the object, and  $i$  is an arbitrary integer less than  $n$ . With this in place, the image of the object is unchanged if the viewpoint of the image is rotated around the symmetry axis for  $-360i/n$  degree ( $R_{axis}^{-1}$ ). This means that the single 2D image of the  $n$ -fold 3D symmetrical object is equivalent to  $n$  images of the same object seen from different viewpoints around the symmetry axis of the object. Those additional images are

called “virtual images” (Vetter & Poggio, 1994) and the 3D shape of the object can be recovered from the original and virtual images by using Multiple-view geometry (Vetter & Poggio, 1994; Hong, Yang, Huang, & Ma, 2004; Yang, Huang, Rao, Hong, & Ma, 2005).

The second method uses the properties of the image of a 3D symmetrical object (see 3.1.1. and 3.2.1.1.). Under an orthographic projection, we assume that projections of the symmetry axis, symmetry polygons, and their CoGs are given. Under a perspective projection, the vanishing point of the symmetry axis is also given. This recovery method can connect a process for detecting 3D symmetry of the object based on its image properties (see 3.2.1.; 3.2.4, see also 3.2.3.) with the recovery process of its 3D shape. We will now show how the 3D shape of a symmetrical object can be recovered from its 2D image under both orthographic and perspective projections.

**3.2.2.1. 3D recovery under a 2D orthographic projection:** Consider the recovery of the 3D shape of a symmetrical object from its 2D orthographic image. Projections of the symmetry axis and the symmetry polygons of the object are assumed to be given in the image (see 3.1.1. and 3.2.1.1.). Set the 2D and 3D Cartesian coordinate systems so that the  $x$ - and  $X$ -axes coincide with the projection of the symmetry axis. When this is done, the symmetry axis should be on the  $ZX$ -plane of the 3D coordinate system:

$$X\cos\theta_{axis} - Z\sin\theta_{axis} + d_{axis} = 0, Y = 0 \quad (2)$$

where  $\theta_{axis}$  is an angle between the symmetry axis and the  $Z$ -axis (a normal to  $\Pi$ ) and  $d_{axis}$  is a constant. The constant  $d_{axis}$  can be arbitrary and it determines the depth position of a 3D shape recovered in the following process. The symmetry axis (2) is normal to a plane:

$$X\sin\theta_{axis} + Z\cos\theta_{axis} - \frac{X_x}{\sin\theta_{axis}} - \frac{d_{axis}}{\tan\theta_{axis}} = 0 \quad (3)$$

where  $X_x$  is an arbitrary real number and the plane (3) intersects with the symmetry axis (2) at:

$$\left[ X_x \quad 0 \quad \frac{X_x}{\tan\theta_{axis}} + \frac{d_{axis}}{\sin\theta_{axis}} \right]^T \quad (4)$$

Consider  $n = 2$ . The symmetry polygons are line-segments (symmetry line-segments) and their CoGs (midpoints) project to midpoints of the projections of the symmetry line-segments. The projections of the midpoints are collinear along the projection of the symmetry axis. Then, projections of vertices of a symmetry line-segment  $i$  can be written as:

$$\left[ x_{mi} \pm x_{di}/2 \quad \pm y_i \right]^T \quad (5)$$

where double-sign corresponds and the midpoint of the projection of the symmetry line-segment  $i$  is  $[x_{mi} \ 0]^T$ . Note that the midpoint of every symmetry line-segment is on the symmetry axis. From equation (2), the midpoint of the symmetry line-segment  $i$  is:

$$[X_{Mi} \ Y_{Mi} \ Z_{Mi}]^T = \left[ x_{mi} \ 0 \ \frac{x_{mi}}{\tan\theta_{axis}} + \frac{d_{axis}}{\sin\theta_{axis}} \right]^T \quad (6)$$

Since every symmetry line-segment is perpendicular to the symmetry axis, the symmetry line segment  $i$  is on the plane (3) when  $X_x = x_{mi}$ . Then, the two vertices of the symmetry line-segment  $i$  can be recovered as:

$$\left[ x_{mi} \pm \frac{x_{di}}{2} \quad \pm y_i \quad \frac{x_{mi}}{\tan\theta_{axis}} + \frac{d_{axis}}{\sin\theta_{axis}} \mp \frac{x_{di}}{2} \tan\theta_{axis} \right]^T \quad (7)$$

where double-signs correspond to one another. Note that  $\theta_{axis}$  is a free parameter that changes the aspect ratio of the recovered 3D shape. From equations (6) and (7), the height of the recovered shape along the symmetry axis changes as a function of  $1/\tan\theta_{axis}$  and the width of the shape changes as a function of  $\tan\theta_{axis}$  along a line that is perpendicular to the symmetry axis and is on the  $XZ$ -plane.

If  $n > 2$ , an equation similar to equation (7) can be applied to the 2D projections of the symmetry polygons for recovering the 3D rotational-symmetrical shape:

$$\left[ x_{gi} + x_{pij} \quad y_{pij} \quad \frac{x_{gi}}{\tan\theta_{axis}} + \frac{d_{axis}}{\sin\theta_{axis}} - x_{pij} \tan\theta_{axis} \right]^T \quad (8)$$

where  $[x_{gi} \ 0]^T$  is the projection of the center of gravity of the symmetry polygon  $i$  and  $[x_{gi} + x_{pij} \ y_{pij}]^T$  is the projection of the  $j$ -th vertex of  $i$ . If  $n > 2$ , the CoGs of the symmetry polygons are used instead of the midpoints of the symmetry line-segments. Note that  $\theta_{axis}$  is no longer a free parameter. Recall that all of the symmetry polygons of the 3D rotational symmetrical shape are regular  $n$ -sided polygons. There exists a unique  $\theta_{axis}$  that makes *all* of the recovered symmetry polygons of the 3D shape regular for a given 2D image of a 3D rotational-symmetrical shape.

**3.2.2.2. 3D recovery under a 2D perspective projection:** With a perspective projection, it is not necessary to distinguish the  $n = 2$  and  $n > 2$  conditions. Now consider the recovery of the 3D shape of a symmetrical object from its 2D perspective image. Projections of the symmetry axis and symmetry polygons of the object are assumed to be given in the image (see 3.1.1. and 3.2.1.1.). Also assume that the vanishing point of the symmetry axis and the projections of the CoGs of the symmetry polygons are given. Now, let the projection of the symmetry axis be  $l_{axis}$  and the vanishing point of the symmetry axis be  $v_{axis}$ . Set the orientation of the 2D  $xy$  Cartesian coordinate system so that  $v_{axis}$  is on the  $x$ -axis,  $v_{axis} =$

$[x_{axis} \ 0]^T$ . Let the  $j$ -th vertex of the  $i$ -th symmetry polygon be  $P_{ij} = [X_{ij} \ Y_{ij} \ Z_{ij}]^T$ , a projection of  $P_{ij}$  be  $p_{ij} = [x_{ij} \ y_{ij}] = [fX_{ij}/Z_{ij} \ fY_{ij}/Z_{ij}]^T$ , its CoG be  $G_i$ , and a projection of  $G_i$  be  $g_i = [x_{gi} \ y_{gi}]^T$ . The symmetry axis is parallel to a line connecting the center of projection  $F = [0 \ 0 \ 0]^T$  and  $v_{axis} = [x_{axis} \ 0 \ f]^T$ . Note that  $G_i$  is on the symmetry axis and  $g_i$  is on  $I_{axis}$ . Once this is established, the projection of the CoG  $G_i$  of the  $i$ -th symmetry polygon can be written as  $g_i = [x_{gi} \ y_{gi}]^T = v_{axis} + r_{gi}[\cos \alpha_{axis} \ \sin \alpha_{axis}]^T$ , where  $r_{gi}$  is the distance from  $v_{axis}$  to  $g_i$  and  $\alpha_{axis}$  is an angle between  $I_{axis}$  and the  $x$ -axis.

Now, consider making the symmetry axis normal to  $\Pi_I$  and all of the symmetry polygons frontoparallel by rotating the camera. This rotation is around the center of projection  $F$  and the image plane  $\Pi_I$  and its 2D coordinate system are rotated together with the camera. Let the camera's rotation be  $R_v$ . Note that the symmetry axis is parallel to a line connecting  $F$  and  $v_{axis}$ , and  $v_{axis}$  is on the  $x$ -axis. It follows that the orientation of the symmetry axis relative to the  $Z$ -axis is  $\sigma_v = \text{atan}(x_{axis}/f)$ . The symmetry axis becomes normal to  $\Pi_I$  by rotating the camera around the  $Y$ -axis for  $\sigma_v$  (Figure 10):  $R_v = R_Y(\sigma_v)$ . The 2D image after  $R_v$  can be computed directly by transforming the 2D image before  $R_v$  (Kanatani, 1988):

$$\begin{cases} x' = f \frac{x \cos \sigma_v - f \sin \sigma_v}{x \sin \sigma_v + f \cos \sigma_v} \\ y' = f \frac{y}{x \sin \sigma_v + f \cos \sigma_v} \end{cases} \quad (9)$$

where  $[x \ y]^T$  is a projection of a point in the 3D scene to  $\Pi_I$  before  $R_v$  and  $[x' \ y']^T$  is its projection after  $R_v$ . Equation (9) can also be represented as follows:

$$\begin{bmatrix} x'^* \\ y'^* \\ w'^* \end{bmatrix} = \begin{pmatrix} f & 0 & 0 \\ 0 & f & 0 \\ 0 & 0 & 1 \end{pmatrix} R_Y^T(\sigma_v) \begin{bmatrix} x \\ y \\ f \end{bmatrix} \quad (10)$$

where  $[x \ y \ f]^T$  and  $[x'^* \ y'^* \ w'^*]^T$  are the homogeneous coordinates of  $[x \ y]^T$  and  $[x' \ y']^T$ . This equation, which represents a rotation of the camera by  $R_v (= R_Y(\sigma_v))$ , is equivalent to rotating the 3D scene by  $R_v^T$ . After this transformation, the vanishing point of the symmetry axis is located at the origin  $[0 \ 0]^T$ , and the projection  $g_i$  of the center of gravity  $G_i$  is transformed to:

$$g'_i = \begin{bmatrix} x'_{gi} \\ y'_{gi} \end{bmatrix} = \frac{r_{gi} f \sin \sigma_v}{r_{gi} \cos \alpha_{axis} \sin^2 \sigma_v - x_{axis}} \begin{bmatrix} \cos \alpha_{axis} \cos \sigma_v \\ \sin \alpha_{axis} \end{bmatrix} \quad (11)$$

The projections of the centers of gravity of the symmetry polygons are still collinear after the transformation along a half-line  $I'_{axis}$  that is the transformation of  $I_{axis}$ . The half-line  $I'_{axis}$  emanates from the origin and the angle of  $I'_{axis}$ , which is measured relative to the direction of the  $x$ -axis, is  $\alpha'_{axis} = \tan^{-1}(\tan \alpha_{axis} / \cos \sigma_v)$ .

The symmetry axis becomes perpendicular to the image plane  $\Pi_I$  after the camera is rotated. This occurs because a line connecting the center of projection and the vanishing point ( $[0 \ 0]^T$ ) in the image is perpendicular to  $\Pi_I$  after the camera is rotated and it is parallel to the symmetry axis. Based on this fact, the center of gravity  $G'_i$  of the symmetry polygon  $i$  after the rotation, can be recovered as:

$$\left[ D_{axis} \cos \alpha'_{axis} \quad D_{axis} \sin \alpha'_{axis} \quad \frac{f D_{axis}}{r'_i} \right]^T \quad (12)$$

where  $D_{axis}$  is a free parameter and  $r'_{gi} = \|g'_i\|$ . The symmetry polygons are parallel to the image plane  $\Pi_I$  after the rotation  $R_v$  and their  $Z$ -coordinates are equal to those of their individual CoGs. At this point, the  $j$ -th vertex of the  $i$ -th symmetry polygon

$P'_{ij} = [X'_{ij} \ Y'_{ij} \ Z'_{ij}]^T$  after the rotation can be recovered from its perspective projection

$P'_{ij} = [X'_{ij} \ Y'_{ij}]^T$  as:

$$P'_{ij} = [X'_{ij} \ Y'_{ij} \ Z'_{ij}]^T = \frac{D_{axis}}{r'_i} [x'_{ij} \ y'_{ij} \ f]^T \quad (13)$$

The free parameter  $D_{axis}$  determines the size of the recovered 3D shape and the distance between the principal axis (the  $Z$ -axis) and the symmetry axis. Recall that the camera's rotation  $R_v$  is equivalent to the rigid rotation  $R_v^T$  of the 3D scene, so the vertex  $P_{ij}$  before the camera's rotation  $R_v$ , can be derived by applying the rotation  $R_v = R_v^{TT}$  to  $P'_{ij}$ :  $P_{ij} = R_v P'_{ij}$ . It is worth pointing out that the perspective projections of the symmetry polygons to  $\Pi_I$  after the camera's rotation  $R_v$  are *regular*  $n$ -sided polygons because the symmetry polygons are regular and they are frontoparallel after the rotation.

**3.2.3. Any pair of 2D curves is consistent with a 3D rotational-symmetrical interpretation**—3D symmetry of an object has to be detected first from its 2D image to recover a 3D shape of the object using its symmetry. However, the symmetry detection is, at least, very difficult. Consider 3D mirror-symmetry. It is almost always possible to find a 3D mirror-symmetrical interpretation of any arbitrary image. Specifically, for a given pair of arbitrary curves in a 2D image, there is always a 3D mirror-symmetrical pair of curves that projects to the given curves under quite general assumptions (Sawada, Li, & Pizlo, 2011, 2014; Hong, Ma, & Yu, 2004). We proved that this is also true for 2-fold, 3D rotational-symmetry. Specifically, there exists a 2-fold, 3D rotational-symmetrical interpretation of a pair of arbitrary curves in a 2D image as well under some general assumptions.

The gist of this proof is as follows: when a pair of curves in a 2D image is given, a set of pairs of lines for establishing correspondence between these curves is the first thing that is determined. The corresponding pairs of points are determined uniquely as the intersections of these lines with the curves. Under an orthographic projection, it is always possible to find

a one-parameter family of its 2-fold 3D symmetrical interpretation around a common symmetry axis for any corresponding pair of 2D points. The family is controlled by the angle between the symmetry axis and a normal to the image plane. Next, under a perspective projection, it is always possible to find its unique 3D symmetrical interpretation around a common symmetry axis for any corresponding pair of 2D points. We will consider a *special* perspective projection before we generalize it to a *general* perspective projection.

### 3.2.3.1. A 3D symmetrical interpretation under a 2D orthographic projection

**Theorem-A1.:** Let  $\phi$  and  $\psi$  be curves in a 2D image. Assume that four lines  $l_{\phi 1}$ ,  $l_{\phi 2}$ ,  $l_{\psi 1}$ , and  $l_{\psi 2}$  that satisfy the following properties can be drawn in the image: (i)  $l_{\phi 1} \parallel l_{\phi 2} \parallel l_{\psi 1} \parallel l_{\psi 2}$ , (ii)  $l_{\phi 1}$  and  $l_{\phi 2}$ , do not intersect with  $\phi$  but do share points with  $\phi$  individually (by being tangent to  $\phi$  or passing the endpoints or non-differentiable points of  $\phi$ ), (iii)  $l_{\psi 1}$  and  $l_{\psi 2}$  do not intersect with  $\psi$  but do share points with  $\psi$  individually, and (iv) a distance between  $l_{\phi 1}$  and  $l_{\phi 2}$  is equal to that between  $l_{\psi 1}$  and  $l_{\psi 2}$  (see Figure 11). Then, there exists a one parameter family of a pair of curves  $\Phi$  and  $\Psi$  in 3D space such that  $\Phi$  and  $\Psi$  are 2-fold rotationally-symmetrical with a symmetry axis  $A_s$  and that  $\phi$  is an orthographic projection of  $\Phi$ , and  $\psi$  is an orthographic projection of  $\Psi$ .

**Proof:<sup>5</sup>** In order to prove this theorem, we must show how the correspondence between  $\phi$  and  $\psi$  is established, and how a corresponding pair of points on  $\phi$  and  $\psi$  can be back-projected in 3D space, such that these back-projected points are symmetrical with respect to the same symmetry axis  $A_s$ . Put simply, the line-segment connecting the back-projected points is bisected by  $A_s$  and is perpendicular to  $A_s$ .

The 2D  $xy$  Cartesian coordinate system on the image plane  $\Pi_I$  is set so that the  $x$ -axis is parallel to the lines  $l_{\phi 1}$ ,  $l_{\phi 2}$ ,  $l_{\psi 1}$ , and  $l_{\psi 2}$  and it is coincident with their midline. The lines  $l_{\phi 1}$ ,  $l_{\phi 2}$ ,  $l_{\psi 1}$ , and  $l_{\psi 2}$  can be written as  $y = y_{l_{\phi 1}}$ ,  $y = y_{l_{\phi 2}}$ ,  $y = y_{l_{\psi 1}}$ , and  $y = y_{l_{\psi 2}}$ , respectively. Without loss of generality, assume that  $y_{l_{\phi 1}} > y_{l_{\phi 2}}$  and  $y_{l_{\psi 1}} < y_{l_{\psi 2}}$ . Then,  $y_{l_{\phi 1}} - y_{l_{\phi 2}} = y_{l_{\psi 2}} - y_{l_{\psi 1}}$ ,  $0 = y_{l_{\phi 1}} + y_{l_{\psi 1}}$ , and  $0 = y_{l_{\phi 2}} + y_{l_{\psi 2}}$ . The  $y$ -coordinate of any point on  $\phi$  is between  $y_{l_{\phi 1}}$  and  $y_{l_{\phi 2}}$  and that of any point on  $\psi$  is between  $y_{l_{\psi 1}}$  ( $= -y_{l_{\phi 1}}$ ) and  $y_{l_{\psi 2}}$  ( $= -y_{l_{\phi 2}}$ ).

Consider a point  $p_i = [x_{\phi i} \ y_{\phi i}]^T$  on  $\phi$  where  $y_{l_{\phi 2}} < y_{\phi i} < y_{l_{\phi 1}}$ . This point should correspond with the point  $q_i = [x_{\psi i} \ y_{\psi i}]^T$  that is an intersection of  $\psi$  with a line  $y = -y_{\phi i}$  where  $y_{l_{\psi 2}} < -y_{\phi i} < y_{l_{\psi 1}}$ . When this is done, their midpoint  $m_i$  is on the  $x$ -axis:  $m_i = [x_{\phi i}/2 + x_{\psi i}/2 \ 0]^T$ . Note that under the orthographic projection, a 3D point  $[X \ Y \ Z]^T$  projects to a point  $[X \ Y]^T$  in the 2D image. It follows that  $P_i = [X_{\phi i} \ Y_{\phi i} \ Z_{\phi i}]^T = [x_{\phi i} \ y_{\phi i} \ Z_{\phi i}]^T$ , and  $Q_i = [X_{\psi i} \ Y_{\psi i} \ Z_{\psi i}]^T = [x_{\psi i} \ -y_{\phi i} \ Z_{\psi i}]^T$  project to  $p_i$  and  $q_i$ , individually.

Recall that  $P_i$  and  $Q_i$  are 3D symmetrical with respect to  $A_s$ , if and only if, they satisfy the following two requirements: i) the line segment connecting  $P_i$  and  $Q_i$  intersects with  $A_s$  at a midpoint  $M_i$  of the segment, and ii) is perpendicular to  $A_s$ . A midpoint  $M_i$  between  $P_i$  and  $Q_i$  is an invariant of the orthographic projection and projects to the midpoint  $m_i$  between  $p_i$  and  $q_i$ . The  $Y$ -coordinate of  $M_i$  is 0 because that of  $m_i$  is also 0. Hence,  $A_s$  is on the  $ZX$ -plane of the 3D coordinate system and can be written as:

<sup>5</sup>A special case of Theorem-A1 that the 2D curves  $\phi$  and  $\psi$  form a closed 2D curve was proved in Sugihara (2016).

$$X \cos \theta_{axis} - Z \sin \theta_{axis} + d_{axis} = 0, Y = 0 \quad (14)$$

where  $\theta_{axis}$  is an angle between the symmetry axis  $A_s$  and the  $Z$ -axis and  $d_{axis}$  is a constant. The line segment connecting  $P_i$  and  $Q_i$  satisfies the requirements i) and ii) of 3D symmetry if:

$$\begin{bmatrix} \sin \theta_{axis} & 0 \cos \theta_{axis} \end{bmatrix} (P_i - Q_i) = 0 \quad (15)$$

$$\begin{bmatrix} \cos \theta_{axis} & 0 & -\sin \theta_{axis} \end{bmatrix} \frac{P_i + Q_i}{2} = -d_{axis} \quad (16)$$

From (15) and (16), we have:

$$P_i = \begin{bmatrix} x_{\phi i} & y_{\phi i} & \frac{x_{\psi i} + x_{\phi i} \cos 2\theta_{axis}}{\sin 2\theta_{axis}} + \frac{d_{axis}}{\sin \theta_{axis}} \end{bmatrix}^T \quad (17)$$

$$Q_i = \begin{bmatrix} x_{\psi i} & -y_{\psi i} & \frac{x_{\psi i} + x_{\phi i} \cos 2\theta_{axis}}{\sin 2\theta_{axis}} + \frac{d_{axis}}{\sin \theta_{axis}} \end{bmatrix}^T \quad (18)$$

Note that  $\theta_{axis}$  is a free parameter; it can be arbitrary, except for  $\sin 2\theta_{axis} = 0$ . So, the 3D interpretations of the 2D curves  $\phi$  and  $\psi$  form a one-parameter family characterized by  $\theta_{axis}$ . The constant  $d_{axis}$  determines the depth positions of the 3D interpretations but does not affect their shapes. Equations (17) and (18) imply that the one-parameter family of the 3D symmetrical interpretations  $\Phi$  and  $\Psi$  of the 2D curves  $\phi$  and  $\psi$  *always* exist.

QED

In the proof of Theorem-A1 above, it was assumed that correspondences between the points of the 2D curves  $\phi$  and  $\psi$  are unique. The case with non-unique correspondences was not considered. Even if the correspondences are not unique, the 3D symmetrical interpretations  $\Phi$  and  $\Psi$  of the 2D curves  $\phi$  and  $\psi$  *always* exist, and they are a pair of continuous curves (Figure 12). Each corresponding pair of points on  $\phi$  and  $\psi$  under the orthographic projection is always established by a pair of lines that are parallel to the  $x$ -axis, and equally distant from the  $x$ -axis. Consider reflecting  $\psi$  about the  $x$ -axis. Then, the lines  $l_{\phi 1}$  and  $l_{\phi 2}$  that are parallel to the  $x$ -axis share points with both  $\phi$  and the 180° rotation of  $\psi$  ( $\psi^{-1}$ ) but they do not intersect with them (see condition (ii) of Theorem-A1). Then, the corresponding points of  $\phi$  and  $\psi^{-1}$  can be connected by a single line parallel to the  $x$ -axis (and  $l_{\phi 1}$  and  $l_{\phi 2}$ , Figure 13). The correspondence is unique only if the line intersects only once with  $\phi$  and  $\psi^{-1}$ .

individually (Figure 13A). This is equivalent to using a way to establish the correspondence between a pair of 2D curves for their 3D mirror-symmetrical interpretations (Sawada, Li, & Pizlo, 2011; see also Rothwell, 1995; Hong, Ma, & Yu, 2004 for a perspective projection). Even if the correspondence between the 2D curves is not always unique, it has been formally proved that the correspondence can be established so that the 3D mirror-symmetrical interpretations are a pair of continuous curves (Theorem 3 in Sawada et al., 2011). The same method can be applied here to establish the correspondence between  $\varphi$  and  $\psi^{-1}$  under the orthographic projection so that  $\Phi$  and  $\Psi$  are a pair of continuous curves.

Assuming that the symmetry axis of a 3D interpretation is perpendicular to the image plane under a perspective projection, the correspondence between a pair of 2D curves is established by a pair of lines that are parallel to the  $x$ -axis as well as under the orthographic projection. This special case in a perspective projection, will be discussed in the next section, and the general perspective projection will be considered on the basis of the special case in the following section.

### 3.2.3.2. A 3D symmetrical interpretation under a 2D special perspective projection

**Lemma-for-Theorem-A2.:** Let  $\varphi$  and  $\psi$  be curves in a 2D image. Assume that four lines  $I_{\varphi 1}$ ,  $I_{\varphi 2}$ ,  $I_{\psi 1}$ , and  $I_{\psi 2}$  that satisfy the following properties can be drawn in the image: (i)  $I_{\varphi 1} \parallel I_{\varphi 2} \parallel I_{\psi 1} \parallel I_{\psi 2}$ , (ii)  $I_{\varphi 1}$  and  $I_{\varphi 2}$  do not intersect with  $\varphi$ , but do share points with  $\varphi$  individually (by being tangent to  $\varphi$  or passing the endpoints or non-differentiable points of  $\varphi$ ), (iii)  $I_{\psi 1}$  and  $I_{\psi 2}$  do not intersect with  $\psi$ , but do share points with  $\psi$  individually, (iv) the midline between  $I_{\varphi 1}$  and  $I_{\psi 1}$  coincide with the midline between  $I_{\varphi 2}$  and  $I_{\psi 2}$ , and (v) the principal point is on the midline (see Figure 14). Then, for a given center of projection  $F$  there exists a pair of curves  $\Phi$  and  $\Psi$  in 3D space such that  $\Phi$  and  $\Psi$  are 2-fold rotationally-symmetrical with respect to a symmetry axis  $A_s$  which is normal to the image plane, and that  $\varphi$  is a perspective projection of  $\Phi$  and  $\psi$  is a perspective projection of  $\Psi$ .

**Proof:** Set the  $x$ -axis of the 2D coordinate system of the image plane  $\Pi_I$  to be parallel to  $I_{\varphi 1}$ ,  $I_{\varphi 2}$ ,  $I_{\psi 1}$ , and  $I_{\psi 2}$  and the  $X$ -axis of the 3D coordinate system to be parallel to the  $x$ -axis. When this is done, the  $x$ -axis coincides with the midline between  $I_{\varphi 1}$  and  $I_{\psi 1}$ , and between  $I_{\varphi 2}$  and  $I_{\psi 2}$  because of condition (v) in the Lemma-for-Theorem-A2. The lines  $I_{\varphi 1}$ ,  $I_{\varphi 2}$ ,  $I_{\psi 1}$ , and  $I_{\psi 2}$  can be written as  $y = y_{I_{\varphi 1}}$ ,  $y = y_{I_{\varphi 2}}$ ,  $y = y_{I_{\psi 1}}$ , and  $y = y_{I_{\psi 2}}$ , respectively. Note that  $y_{I_{\varphi 1}} - y_{I_{\varphi 2}} = y_{I_{\psi 2}} - y_{I_{\psi 1}}$ ,  $0 = y_{I_{\varphi 1}} + y_{I_{\psi 1}}$ , and  $0 = y_{I_{\varphi 2}} + y_{I_{\psi 2}}$ . Then, the  $y$ -coordinate of any point on  $\varphi$  is between  $y_{I_{\varphi 1}}$  and  $y_{I_{\varphi 2}}$ , and the  $y$ -coordinate of any point on  $\psi$  is between  $y_{I_{\psi 1}}$  and  $y_{I_{\psi 2}}$ .

Now consider a point  $p_i = [x_{\varphi i} \ y_{\varphi i}]^T$  on  $\varphi$  where  $y_{I_{\varphi 2}} < y_{\varphi i} < y_{I_{\varphi 1}}$ . This point should correspond with a point  $q_i = [x_{\psi i} \ y_{\psi i}]^T$  that is an intersection of  $\psi$  with a line  $y = -y_{\varphi i}$  where  $y_{I_{\psi 2}} < -y_{\varphi i} < y_{I_{\psi 1}}$ . Then, the midpoint  $m_i$  of  $p_i$  and  $q_i$  is on the  $x$ -axis:  $m_i = [(x_{\varphi i} + x_{\psi i})/2 \ 0]^T$ . Under a perspective projection, a 3D point  $[X \ Y \ Z]^T$  projects to an image point  $[fX/Z \ fY/Z]^T$ , so  $P_i = [X_{\varphi i} \ Y_{\varphi i} \ Z_{\varphi i}]^T = [x_{\varphi i}Z_{\varphi i}/f \ y_{\varphi i}Z_{\varphi i}/f \ Z_{\varphi i}]^T$  and  $Q_i = [X_{\psi i} \ Y_{\psi i} \ Z_{\psi i}]^T = [x_{\psi i}Z_{\psi i}/f \ -y_{\varphi i}Z_{\psi i}/f \ Z_{\psi i}]^T$  project to  $p_i$  and  $q_i$  individually.

Recall that  $P_i$  and  $Q_i$  are 3D symmetrical with respect to the symmetry axis  $A_s$ , if and only if, they satisfy the following two requirements: (i) the line-segment connecting  $P_i$  and  $Q_i$  intersects with  $A_s$  at a midpoint  $M_i$  of the segment, and (ii) it is perpendicular to  $A_s$ . The line-segment connecting  $P_i$  and  $Q_i$  is also perpendicular to the normal of the image plane  $\Pi_I$  because  $A_s$  is parallel to the normal of  $\Pi_I$ . Under this condition, a midpoint  $M_i$  between  $P_i$  and  $Q_i$  projects to the midpoint  $m_i$  between  $p_i$  and  $q_i$ . The  $Y$ -coordinate of  $M_i$  is 0 because the  $y$ -coordinate of  $m_i$  is also 0. So,  $A_s$  can be written as:

$$X = X_{axis}, Y = 0 \quad (19)$$

where  $X_{axis}$  represents the  $X$ -coordinate of an intersection of  $A_s$  with the  $x$ -axis. Since  $M_i$  is on  $A_s$ :

$$M_i = \left[ X_{axis} \quad 0 \quad \frac{2fX_{axis}}{x_{\varphi i} + x_{\psi i}} \right]^T \quad (20)$$

The  $Z$ -coordinate of  $M_i$  is the same as those of  $P_i$  and  $Q_i$  because the line-segment connecting  $P_i$  and  $Q_i$  is perpendicular to a normal of the image plane  $\Pi_I$ . From (20), we have:

$$P_i = \left[ \frac{2x_{\varphi i}X_{axis}}{x_{\varphi i} + x_{\psi i}} \quad \frac{2y_{\varphi i}X_{axis}}{x_{\varphi i} + x_{\psi i}} \quad \frac{2fX_{axis}}{x_{\varphi i} + x_{\psi i}} \right]^T \quad (21)$$

$$Q_i = \left[ \frac{2x_{\varphi i}X_{axis}}{x_{\varphi i} + x_{\psi i}} \quad \frac{-2y_{\varphi i}X_{axis}}{x_{\varphi i} + x_{\psi i}} \quad \frac{2fX_{axis}}{x_{\varphi i} + x_{\psi i}} \right]^T \quad (22)$$

Equations (21) and (22) imply that the 3D rotationally-symmetrical interpretation  $\Phi$  and  $\Psi$  of the 2D curves  $\varphi$  and  $\psi$  always exists. They diverge to infinity if  $x_{\varphi i} + x_{\psi i} = 0$  and are not tame (see 2. Definition). Note that  $X_{axis}$  changes the size of  $\Phi$  and  $\Psi$  but does not affect their shapes.

QED

Based on the Lemma-for-Theorem-A2, we will consider establishing symmetry correspondence in a 2D image under a *general* perspective projection. Recall that the correspondence between a pair of 2D curves was established for the lemma by a pair of parallel lines whose midline passes the principal point. Under the *general* perspective projection, correspondence is established by a pair of half-lines that emanate from a point in an image.

### 3.2.3.3. A 3D symmetrical interpretation under a 2D general perspective projection

**Theorem-A2.:** Let a center of projection  $F$  be  $[0\ 0\ 0]^T$ , a 2D image plane  $\Pi_I$  be  $Z = f$ , and  $\varphi$  and  $\psi$  be curves in  $\Pi_I$ . Assume that four half-lines  $I_{\varphi 1}$ ,  $I_{\varphi 2}$ ,  $I_{\psi 1}$ , and  $I_{\psi 2}$ , which satisfy the following three properties, can be drawn in the image: (i) endpoints of all of the half-lines are at a point  $v_c$ , that is, not on  $\varphi$  and  $\psi$ , (ii)  $I_{\varphi 1}$  and  $I_{\varphi 2}$  do not intersect with  $\varphi$ , but do share points with  $\varphi$  individually (by being tangent to  $\varphi$  or passing the endpoints or non-differentiable points of  $\varphi$ ), (iii)  $I_{\psi 1}$ , and  $I_{\psi 2}$  do not intersect with  $\psi$  but do share points with  $\psi$ , individually (see Figure 15). Now let the 2D  $xy$  Cartesian coordinate system be set so that the origin is at the principal point in the image and  $v_c$  is on the  $x$ -axis:  $v_c = [x_c\ 0]^T$ . Let a line  $h_c$  be  $x = -f/z_c$  and its intersection with  $I_{\varphi 1}$ ,  $I_{\varphi 2}$ ,  $I_{\psi 1}$ , and  $I_{\psi 2}$  be  $u_{\varphi 1}$ ,  $u_{\varphi 2}$ ,  $u_{\psi 1}$ , and  $u_{\psi 2}$  respectively. Then, additionally assume (iv)  $x_{\varphi\psi}/x_c < 1$  where  $x_{\varphi\psi}$  is the  $x$  coordinate of any point on  $\varphi$  and  $\psi$  and (v) an angle bisector of  $\angle U_{\varphi 1} F U_{\psi 1}$  coincides with that of  $\angle U_{\varphi 2} F U_{\psi 2}$  where  $U_{\varphi 1} = [u_{\varphi 1}\ f]^T$ ,  $U_{\psi 1} = [u_{\psi 1}\ f]^T$ ,  $U_{\varphi 2} = [u_{\varphi 2}\ f]^T$ , and  $U_{\psi 2} = [u_{\psi 2}\ f]^T$ . With this done, there exists a pair of curves  $\Phi$  and  $\Psi$  in a 3D space such that  $\Phi$  and  $\Psi$  are 2-fold rotationally-symmetrical with respect to a symmetry axis  $A_s$  and  $\varphi$  is a perspective projection of  $\Phi$ , and  $\psi$  is a perspective projection of  $\Psi$ .

**Proof:** In order to prove this theorem,  $\varphi$  and  $\psi$  are transformed to  $\varphi''$  and  $\psi''$  by simulating a camera rotation  $R_c$  (Kanatani, 1988) around the center of projection  $F$  so that  $\varphi''$  and  $\psi''$  satisfy the conditions of the Lemma-for-Theorem-A2. Condition (iv) of Theorem-A2 should be satisfied so that  $\varphi''$  and  $\psi''$  are a pair of tame curves (see 2. Definition). Conditions (iv) and (v) of the Lemma-for-Theorem-A2 is satisfied for  $\varphi''$  and  $\psi''$  is satisfied if Condition (v) of Theorem-A2 is satisfied. Based on the Lemma-for-Theorem-A2, the 3D symmetrical interpretation  $\Phi''$  and  $\Psi''$  of  $\varphi''$  and  $\psi''$  can be constructed. Then, the 3D symmetrical interpretation  $\Phi$  and  $\Psi$  of  $\varphi$  and  $\psi$  is generated by rotating  $\Phi''$  and  $\Psi''$  by  $R_c$ .

Set the  $x$ -axis of the 2D coordinate system of the image plane  $\Pi_I$  to pass the point  $v_c$  and the  $X$ -axis of the 3D coordinate system to be parallel to the  $x$ -axis (Figure 15). Then, any point in  $\Pi_I$  can be represented in a polar coordinate system and can be written as  $[x\ y]^T = [x_c + r\cos\alpha\ r\sin\alpha]^T$ , where  $r$  is a length of a line-segment between  $[x\ y]^T$  and  $v_c$  and  $\alpha$  is an angle of the segment relative to the direction of the  $x$ -axis. Any point on a half-line that emanates from  $v_c$  can be represented with a constant  $\alpha$ . For example,  $\alpha$  is  $\tan^{-1}(-y_{u_{\varphi 1}}/x_c)$  for  $I_{\varphi 1}$ ,  $\tan^{-1}(-y_{u_{\varphi 2}}/x_c)$  for  $I_{\varphi 2}$ ,  $\tan^{-1}(-y_{u_{\psi 1}}/x_c)$  for  $I_{\psi 1}$ , and  $\tan^{-1}(-y_{u_{\psi 2}}/x_c)$  for  $I_{\psi 2}$  where  $y_{u_{\varphi 1}}$ ,  $y_{u_{\varphi 2}}$ ,  $y_{u_{\psi 1}}$ , and  $y_{u_{\psi 2}}$  are  $y$ -coordinates of  $u_{\varphi 1}$ ,  $u_{\varphi 2}$ ,  $u_{\psi 1}$ , and  $u_{\psi 2}$ . Then,  $\alpha$  is between  $\tan^{-1}(-y_{u_{\varphi 1}}/x_c)$  and  $\tan^{-1}(-y_{u_{\varphi 2}}/x_c)$  inclusive for any point on  $\varphi$  and between  $\tan^{-1}(-y_{u_{\psi 1}}/x_c)$  and  $\tan^{-1}(-y_{u_{\psi 2}}/x_c)$  inclusive for that on  $\psi$ .

A 3D rotationally-symmetrical interpretation  $\Phi$  and  $\Psi$  of the 2D curves  $\varphi$  and  $\psi$  will be constructed so that the vanishing point  $v_{axis}$  of their symmetry axis is on  $h_c$  and  $v_c$  is on the horizon  $h_{axis}$  of the symmetry axis. The common angle bisector of  $\angle U_{\varphi 1} F U_{\psi 1}$  and  $\angle U_{\varphi 2} F U_{\psi 2}$  intersects with the image plane  $\Pi_I$  at the position of  $v_{axis}$ .

Consider rotating the camera with the image plane  $\Pi_I$  around the center of projection  $F$  to transform  $\varphi$ ,  $\psi$ ,  $I_{\varphi 1}$ ,  $I_{\varphi 2}$ ,  $I_{\psi 1}$ , and  $I_{\psi 2}$  so that their transformations satisfy the conditions of

the Lemma for-Theorem-A2.<sup>6</sup> The image after the rotation can be computed from the image before the rotation as long as the position of the center of projection  $F$  is kept constant in the scene (Kanatani, 1988). The rotation  $R_c$  is done in two steps: the first rotation  $R_{cY}$  around the  $Y$ -axis and the second rotation  $R_{cX}$  around the  $X$ -axis (Figure 16). The first rotation  $R_{cY}$  is  $R_Y(\sigma_{cY})$  where  $\sigma_{cY} = \tan^{-1}(-f/x_c)$ . Then,  $[x\ y]^T = [x_c + r \cos \alpha\ r \sin \alpha]^T$  before  $R_{cY}$  is transformed to (Kanatani, 1988):

$$\begin{bmatrix} \hat{x} \\ \hat{y} \end{bmatrix} = \begin{bmatrix} \frac{x \cos \sigma_{cY} - f \sin \sigma_{cY}}{f \cos \sigma_{cY} + x \sin \sigma_{cY}} \\ \frac{y}{f \cos \sigma_{cY} + x \sin \sigma_{cY}} \end{bmatrix} = \begin{bmatrix} -x_c - \frac{x_c^2 + f^2}{r \cos \alpha} \\ -x_c \frac{\tan \alpha}{\cos \sigma_{cY}} \end{bmatrix} \quad (23)$$

after  $R_{cY}$ . Then,  $u_{\phi_1}$ ,  $u_{\phi_2}$ ,  $u_{\psi_1}$ , and  $u_{\psi_2}$  on  $h_c(x = -f^2/x_c)$  are transformed to  $u_{\phi_1} = [0\ y_{u\phi_1} \cos \sigma_{cY}]^T$ ,  $u_{\phi_2} = [0\ y_{u\phi_2} \cos \sigma_{cY}]^T$ ,  $u_{\psi_1} = [0\ y_{u\psi_1} \cos \sigma_{cY}]^T$ , and  $u_{\psi_2} = [0\ y_{u\psi_2} \cos \sigma_{cY}]^T$  on the  $y$ -axis. Recall that the angle bisector of  $\angle U_{\phi_1} F U_{\psi_1}$  coincides with that of  $\angle U_{\phi_2} F U_{\psi_2}$  (condition (v) of Theorem-A2) before  $R_{cY}$ . Let an intersection of the bisector with  $II$  be  $U_0 = [-f^2/x_c\ y_0\ f]^T$ :  $\angle U_0 F U_{\phi_1} = \angle U_0 F U_{\psi_1}$ , and  $\angle U_0 F U_{\phi_2} = \angle U_0 F U_{\psi_2}$ . After  $R_{cY}$ ,  $u_0 = [-f^2/x_c\ y_0]^T$  is transformed to  $u_0 = [0\ y_0 \cos \sigma_{cY}]^T$ . The second rotation  $R_{cX}$  around the  $X$ -axis is determined so that  $u_0$  is transformed to  $\hat{u}_0 = [0\ 0]^T$  after  $R_{cX}$ :  $R_{cX} = R_X(\sigma_{cX})$  where  $\sigma_{cX} = \tan^{-1}(-y_0 \cos \sigma_{cY} / f)$ . Then, a point  $[x\ y]^T = [x_c + r \cos \alpha\ r \sin \alpha]^T$  before  $R_{cY} R_{cX} (= R_c)$ <sup>7</sup> is projected to (Kanatani, 1988):

$$\begin{bmatrix} \hat{x} \\ \hat{y} \end{bmatrix} = \begin{bmatrix} \frac{\hat{x}}{f \cos \sigma_{cX} - \hat{y} \sin \sigma_{cX}} \\ \frac{f \sin \sigma_{cX} + \hat{y} \cos \sigma_{cX}}{f \cos \sigma_{cX} - \hat{y} \sin \sigma_{cX}} \end{bmatrix} - \frac{f^2}{y_0 x_c \tan \alpha - f^2} \begin{bmatrix} \frac{x \cos \sigma_{cY} + x_c^2 + f^2}{r \cos \alpha \cos \sigma_{cX}} \\ \frac{x_c \tan \alpha + y_0 \cos^2 \sigma_{cY}}{\cos \sigma_{cY}} \end{bmatrix} \quad (24)$$

after  $R_{cY} R_{cX}$ .

Let  $\hat{\phi}$  and  $\hat{\psi}$  be transformations of  $\phi$ ,  $\psi$  and  $\hat{l}_{\phi_1}$ ,  $\hat{l}_{\phi_2}$ ,  $\hat{l}_{\psi_1}$ , and  $\hat{l}_{\psi_2}$  be transformations of  $l_{\phi_1}$ ,  $l_{\phi_2}$ ,  $l_{\psi_1}$ , and  $l_{\psi_2}$  after the camera rotation  $R_c (= R_{cY} R_{cX})$ . All the five conditions of Lemma-for-Theorem-A2 are satisfied by curves  $\hat{\phi}$ , and  $\hat{\psi}$  and lines  $\hat{l}_{\phi_1}$ ,  $\hat{l}_{\phi_2}$ ,  $\hat{l}_{\psi_1}$ , and  $\hat{l}_{\psi_2}$ . From equation (24),  $\hat{y}$  is dependent on  $\alpha$  but is independent from  $r$ . Then,  $\hat{l}_{\phi_1}$ ,  $\hat{l}_{\phi_2}$ ,  $\hat{l}_{\psi_1}$ , and  $\hat{l}_{\psi_2}$  are lines parallel to the  $x$ -axis (the condition (i) of the lemma) because  $l_{\phi_1}$ ,  $l_{\phi_2}$ ,  $l_{\psi_1}$ , and  $l_{\psi_2}$  are represented individually by constant  $\alpha$ . Next, from the conditions (ii) and (iii) of Theorem-A2,  $l_{\phi_1}$  and  $l_{\phi_2}$  do not intersect with  $\phi$ , but do share points with  $\phi$  individually and (iii)  $l_{\psi_1}$  and  $l_{\psi_2}$  do not intersect with  $\psi$  but do share points with  $\psi$  individually. These properties are invariant under the transformation that simulates the camera rotation  $R_c$ . Therefore, the conditions (ii) and (iii) of the Lemma are also satisfied.

<sup>7</sup>A rotation matrix combining the first rotation  $R_{cY}$  and the second rotation  $R_{cX}$  is written as  $R_{cY} R_{cX}$  because the 3D coordinate system rotates when the camera rotates.

Now, consider a midline between  $\varphi_1$  and  $\psi_1$  and that between  $\varphi_2$  and  $\psi_2$ . These midlines are parallel to the  $x$ -axis because  $\varphi_1$ ,  $\varphi_2$ ,  $\psi_1$ , and  $\psi_2$  are. The  $y$ -intercepts of  $\varphi_1$ ,  $\varphi_2$ ,  $\psi_1$ , and  $\psi_2$  are  $u_{\varphi_1} = [0 \tan \angle U_0 F U_{\varphi_1}]^T$ ,  $u_{\varphi_2} = [0 \tan \angle U_0 F U_{\varphi_2}]^T$ ,  $u_{\psi_1} = [0 \tan \angle U_0 F U_{\psi_1}]^T$ , and  $u_{\psi_2} = [0 \tan \angle U_0 F U_{\psi_2}]^T$ , which are transformations of  $u_{\varphi_1}$ ,  $u_{\varphi_2}$ ,  $u_{\psi_1}$ , and  $u_{\psi_2}$  after  $R_c$  via  $u_{\varphi_1}$ ,  $u_{\varphi_2}$ ,  $u_{\psi_1}$ , and  $u_{\psi_2}$ . Note that  $\tan \angle U_0 F U_{\varphi_1} = -\tan \angle U_0 F U_{\psi_1}$ , and  $\tan \angle U_0 F U_{\varphi_2} = -\tan \angle U_0 F U_{\psi_2}$  because  $\angle U_0 F U_{\varphi_1} = -\angle U_0 F U_{\psi_1}$ , and  $\angle U_0 F U_{\varphi_2} = -\angle U_0 F U_{\psi_2}$  (see Supplemental Materials). With this done, the midline between  $\varphi_1$  and  $\psi_1$  and that between  $\varphi_2$  and  $\psi_2$  coincide with the  $x$ -axis. It follows that the conditions (iv) and (v) of the Lemma are also satisfied.

All the conditions of the Lemma-for-Theorem-A2 are satisfied by curves  $\varphi$  and  $\psi$  with lines  $\varphi_1$ ,  $\varphi_2$ ,  $\psi_1$ , and  $\psi_2$ . Therefore, from the Lemma-for-Theorem-A2, a 3D rotationally symmetrical interpretation  $\Phi$  and  $\Psi$  of the 2D curves  $\varphi$  and  $\psi$  always exists. The camera rotation  $R_{cY} R_{cX}$  is equivalent to a rigid rotation of the 3D scene by  $R_{cX}^T R_{cY}^T$  around  $F$  so, the 3D interpretation  $\Phi$  and  $\Psi$  project to  $\varphi$  and  $\psi$  after being rotated by  $R_{cX}^T R_{cY}^T$  around  $F$ .

QED

### 3.2.4. Model-based invariant of 3D rotational-symmetry with planarity of contours

In the previous section we showed that detecting a 2-fold 3D symmetry from a 2D image is an ill-posed problem. Almost any 2D image can be consistent with some 3D symmetrical interpretation. The best (probably the only) way to transform this ill-posed problem to a well-posed problem is by applying an additional constraint.

Now consider 3D mirror-symmetry. There are model-based invariants of 3D mirror symmetry under both orthographic and perspective projections. Under the orthographic projection, lines connecting pairs of corresponding points in the 2D image are parallel to one another. Under the perspective projection, the lines connecting corresponding points converge at a point in the 2D image. These are the only invariants of 3D mirror-symmetry, but additional invariants can be introduced into the image if 3D mirror-symmetry is used along with another constraint, namely with the planarity of contours (Sawada, Li, & Pizlo, 2014). Consider a 3D mirror-symmetrical pair of planar curves. Under the orthographic projection, the relationship between images of the curves can be represented by a sub-group of the 2D affine transformation. Under the perspective projection, the relationship can also be represented by a transformation that includes the same sub-group of the 2D affine transformation. This planarity constraint plays an important role for the human visual system to detect 3D mirror-symmetry from the 2D image (Sawada, Li, & Pizlo, 2011, 2014).

In this section, we will apply the same approach to 3D rotational-symmetry, specifically we will derive transformations among 2D images of a 3D symmetrical set of planar curves under both orthographic (Figure 17) and perspective projections. These transformations are model-based invariants of 3D symmetry taken together with the planarity of contours under those projections.

### 3.2.4.1. Model-based invariant under a 2D orthographic projection

**Theorem-B1.:** Let  $\Phi_{n1}, \Phi_{n2}, \dots, \Phi_{ni}, \dots, \Phi_{nn}$  be an  $n$ -fold 3D symmetrical set of planar curves and  $\varphi_{on1}, \varphi_{on2}, \dots, \varphi_{oni}, \dots, \varphi_{onn}$  be their orthographic projections in a 2D image plane  $\Pi_I$  where  $i$  is a natural number between 1 and  $n$ . Assume that an orthographic projection of their symmetry axis is given. Let us set the 2D  $xy$  Cartesian coordinate system in  $\Pi_I$  so that the projection of the symmetry axis coincides with the  $x$ -axis. Then, the relation between  $\varphi_{on1}$  and  $\varphi_{oni}$  can be represented as follows:

$$R_{2D}(\pi - \zeta_{ni}) \begin{bmatrix} x_{oni} \\ y_{oni} \\ 1 \end{bmatrix} = \begin{pmatrix} m_{11} & m_{12} & m_{13} \\ 0 & 1 & 0 \\ 0 & 0 & 1 \end{pmatrix} R_{2D}(\zeta_{ni}) \begin{bmatrix} x_{on1} \\ y_{on1} \\ 1 \end{bmatrix} \quad (25)$$

$$\zeta_{ni} = \tan^{-1} \frac{\sin(2\pi(i-1)/n)}{(\cos(2\pi(i-1)/n) - 1) \cos \theta_{axis}}$$

where  $p_{on1} = [x_{on1} \ y_{on1}]^T$  and  $p_{oni} = [x_{oni} \ y_{oni}]^T$  are a pair of corresponding points on  $\varphi_{on1}$  and  $\varphi_{oni}$ .  $m_{11}$ ,  $m_{12}$ , and  $m_{13}$  are free parameters, and  $\theta_{axis}$  is an orientation of the symmetry axis relative to a normal of  $\Pi_I$ .

**Proof:** Consider the  $n$ -fold 3D symmetrical set of planar curves  $\Phi_{n1}, \Phi_{n2}, \dots, \Phi_{ni}, \dots, \Phi_{nn}$  where  $i$  is a natural number between 1 and  $n$ . Without loss of any generality, we can assume that its symmetry axis is on the  $XZ$ -plane (see 3.1.1. and 3.2.1.1.). A symmetrical pair of points  $P_{n1}$  and  $P_{ni}$  on  $\Phi_{n1}$  and  $\Phi_{ni}$  can be written as:

$$P_{n1} = R_z(\theta_{axis}) \begin{bmatrix} X_{n1} + D_X \\ Y_{n1} \\ Z_{n1} \end{bmatrix} = \begin{bmatrix} X_{n1} \cos \theta_{axis} + Z_{n1} \sin \theta_{axis} + D_X \cos \theta_{axis} \\ Y_{n1} \\ -X_{n1} \sin \theta_{axis} + Z_{n1} \cos \theta_{axis} - D_X \cos \theta_{axis} \end{bmatrix} \quad (26)$$

$$P_{ni} = R_z(\theta_{axis}) \begin{bmatrix} X_{n1} \cos \theta_{axis} - Y_{n1} \sin \omega_{ni} + D_X \\ X_{n1} \sin \omega_{ni} + Y_{n1} \cos \omega_{ni} \\ Z_{ni} \end{bmatrix} = \quad (27)$$

$$\begin{bmatrix} (X_{n1} \cos \omega_{ni} - Y_{n1} \sin \omega_{ni}) \cos \theta_{axis} + Z_{n1} \sin \theta_{axis} + D_X \cos \theta_{axis} \\ X_{n1} \sin \omega_{ni} + Y_{n1} \cos \omega_{ni} \\ -(X_{n1} \cos \omega_{ni} - Y_{n1} \sin \omega_{ni}) \sin \theta_{axis} + Z_{n1} \cos \theta_{axis} - D_X \sin \theta_{axis} \end{bmatrix}$$

where  $D_X$  and  $\theta_{axis}$  are constants and  $\omega_{ni}$  is  $2\pi(i-1)/n$ . An orthographic projection of the symmetry axis is on the  $x$ -axis and orthographic projections of  $P_{n1}$  and  $P_{ni}$  are:

$$p_{on1} = \begin{bmatrix} x_{on1} \\ y_{on1} \end{bmatrix} = \begin{bmatrix} X_{n1} \cos \theta_{axis} + Z_{n1} \sin \theta_{axis} + D_X \cos \theta_{axis} \\ Y_{n1} \end{bmatrix} \quad (28)$$

$$p_{oni} = \begin{bmatrix} x_{oni} \\ y_{oni} \end{bmatrix} = \begin{bmatrix} (X_{n1} \cos \omega_{ni} - Y_{n1} \sin \omega_{ni}) \cos \theta_{axis} + Z_{n1} \sin \theta_{axis} + D_X \cos \theta_{axis} \\ X_{n1} \sin \omega_{ni} + Y_{n1} \cos \omega_{ni} \end{bmatrix} \quad (29)$$

Then, a pair of points  $\dot{p}_{on1}$  and  $\dot{p}_{oni}$  in the image plane  $\Pi_I$  is computed by rotating  $p_{on1}$  for  $\zeta_{ni}$  and  $p_{oni}$  for  $\pi - \zeta_{ni}$ :

$$\dot{p}_{on1} = R_{2D}(\zeta_{ni})p_{on1} = \quad (30)$$

$$\begin{bmatrix} x_{on1} \cos \zeta_{ni} - y_{on1} \sin \zeta_{ni} \\ \frac{(X_{n1} \cos \theta_{axis} + Z_{n1} \sin \theta_{axis} + D_X \cos \theta_{axis}) \sin \omega_{ni} + (\cos \omega_{ni} - 1) \cos \theta_{axis}}{\sqrt{\sin^2 \omega_{ni} (\cos \omega_{ni} - 1)^2 \cos^2 \theta_{axis}}} \end{bmatrix}$$

$$\dot{p}_{oni} = R_{2D}(\pi - \zeta_{ni})p_{oni} = \quad (31)$$

$$\begin{bmatrix} -x_{oni} \cos \zeta_{ni} - y_{oni} \sin \zeta_{ni} \\ \frac{(X_{n1} \cos \theta_{axis} + Z_{n1} \sin \theta_{axis} + D_X \cos \theta_{axis}) \sin \omega_{ni} + (\cos \omega_{ni} - 1) \cos \theta_{axis}}{\sqrt{\sin^2 \omega_{ni} (\cos \omega_{ni} - 1)^2 \cos^2 \theta_{axis}}} \end{bmatrix}$$

where:

$$\zeta_{ni} = \tan^{-1} \frac{\sin \omega_{ni}}{(\cos \omega_{ni} - 1) \cos \theta_{axis}} \quad (32)$$

Recall that both  $\Phi_{n1}$  and  $\Phi_{ni}$  are individually planar. Each planar curve in a 3D scene is a 2D curve on a plane. Therefore, the orthographic projections  $\phi_{on1}$  and  $\phi_{oni}$  of  $\Phi_{n1}$  and  $\Phi_{ni}$  from

the 3D scene to the 2D image plane  $\Pi_I$  can be represented by 2D orthographic projections from the planes of  $\Phi_{n1}$  and  $\Phi_{ni}$  to  $\Pi_I$  and the 2D orthographic projection is a sub-set of the 2D affine transformation. Then, a relation between the orthographic projections  $\varphi_{on1}$  and  $\varphi_{oni}$  can also be represented by a 2D affine transformation. The  $y$ -coordinates of  $\dot{p}_{on1}$  and  $\dot{p}_{oni}$  are identical to one another in Equations (30) and (31). Therefore, the relation between  $\varphi_{on1}$  and  $\varphi_{oni}$  is represented specifically by a subgroup of the 2D affine transformation:

$$R_{2D}(\pi - \zeta_{ni})p_{oni} = \begin{pmatrix} m_{11} & m_{12} \\ 0 & 1 \end{pmatrix} R_{2D}(\zeta_{ni})p_{on1} + \begin{bmatrix} m_{13} \\ 0 \end{bmatrix} \quad (33)$$

Note that  $m_{11}$ ,  $m_{12}$ , and  $m_{13}$  represent 1D scaling, shear, and translation along the  $x$ -axis between  $\dot{p}_{on1}$  and  $\dot{p}_{oni}$ .

QED

Note that  $\zeta_{ni}$  is 0 and is independent from  $\theta_{axis}$  if  $i = n = 2$ . The slant  $\theta_{axis}$  of the symmetry axis is a free parameter for recovering a 3D shape of a 2-fold symmetrical object from its 2D orthographic image (see 3.2.2.1) and does not affect this relation between  $\varphi_{on1}$  and  $\varphi_{oni}$ . A relation between  $\varphi_{on1}$  and the  $180^\circ$  rotation of  $\varphi_{oni}$  is represented by the 1D scaling, shear, and translation along the  $x$ -axis 805 under this condition (see 3.2.3.1, Figure 13).

It is worth pointing out that the subgroup of the 2D affine transformation in Equation (33) also appears in a transformation representing the relationship between perspective projections of a 3D mirror-symmetrical pair of planar curves (Equation (1) in Sawada, Li, & Pizlo, 2014). But, Equation (33) has two rotation matrices  $R_{2D}(\xi_{ni})$  and  $R_{2D}(\pi - \xi_{ni})$  that do *not* exist in the transformation used for 3D mirror-symmetry. Hence, Equation (33) is more complicated than the transformation for 3D mirror-symmetry.

### 3.2.4.2. Model-based invariant under a 2D special perspective projection

**Lemma-for-Theorem-B2.:** Let  $\Phi_{n1}, \Phi_{n2}, \dots, \Phi_{ni}, \dots, \Phi_{nn}$  be an  $n$ -fold 3D symmetrical set of planar curves and  $\varphi_{on1}, \varphi_{on2}, \dots, \varphi_{oni}, \dots, \varphi_{onn}$  be their perspective projections in the 2D image plane  $\Pi_I$  where  $i$  is a natural number between 1 and  $n$ . Assume that their symmetry axis is perpendicular to  $\Pi_I$  and its perspective projection in  $\Pi_I$  is given. Note that a vanishing point of the symmetry axis appears at the principal point of the perspective projection in  $\Pi_I$ . Let us set the 2D  $xy$  Cartesian coordinate system in  $\Pi_I$  so that the origin is at the principal point and the projection of the symmetry axis coincides with the  $x$ -axis. Then, a relation between  $\varphi_{pn1}$  and  $\varphi_{pni}$  can be represented as follows:

$$R_z(\xi_{ni} - \omega_{ni}) \begin{bmatrix} x_{pni} \\ y_{pni} \\ f \end{bmatrix} = \begin{pmatrix} m_{11} & m_{12} & m_{13} \\ 0 & 1 & 0 \\ 0 & 0 & 1 \end{pmatrix} R_z(\xi_{ni}) \begin{bmatrix} x_{pn1} \\ y_{pn1} \\ f \end{bmatrix} \quad (34)$$

$$\xi_{ni} = \tan^{-1} \frac{\sin \omega_{ni}}{\cos \omega_{ni} - 1}$$

where  $[x_{pn1} \ y_{pn1}]^T$  and  $[x_{pni} \ y_{pni}]^T$  are a pair of corresponding points on  $\Phi_{pn1}$  and  $\Phi_{pni}$  and  $m_{11}$ ,  $m_{12}$ , and  $m_{13}$  are free parameters.

**Proof:** Consider the  $n$ -fold 3D symmetrical set of planar curves  $\Phi_{n1}, \Phi_{n2}, \dots, \Phi_{ni}, \dots, \Phi_{nn}$  with a symmetry axis that is parallel to the  $Z$ -axis and intersects with the  $X$ -axis. A symmetric pair of points  $P_{n1}$  and  $P_{ni}$  on  $\Phi_{n1}$  and  $\Phi_{ni}$  can be written as:

$$P_{n1} = [X_{n1} + D_X \ Y_{n0} \ Z_{n0}]^T \quad (35)$$

$$\begin{aligned} P_{ni} &= [X_{ni} \ Y_{ni} \ Z_{ni}]^T \\ &= [X_{n1} \cos \omega_{ni} - Y_{n1} \sin \omega_{ni} - D_X \ X_{n1} \sin \omega_{ni} + Y_{n0} \cos \omega_{ni} \ Z_{n1}]^T \end{aligned} \quad (36)$$

where  $[D_X \ 0 \ 0]^T$  is the  $X$ -intercept of the symmetry axis. Let  $\varphi_{pn1}$ ,  $\varphi_{pni}$ ,  $p_{pn1}$ , and  $p_{pni}$  be perspective projections of  $\Phi_{n1}$ ,  $\Phi_{ni}$ ,  $P_{pn1}$ , and  $P_{pni}$ :

$$p_{pn1} = \left[ \frac{f(X_{n1} + D_X)}{Z_{n1}} \ \frac{fY_1}{Z_{n1}} \right]^T \quad (37)$$

$$p_{pni} = \left[ \frac{f(X_{n1} \cos \omega_{ni} - Y_{n1} \sin \omega_{ni} - D_X)}{Z_{n1}} \ \frac{f(X_{n1} \sin \omega_{ni} + Y_{n1} \cos \omega_{ni})}{Z_{n1}} \right]^T \quad (38)$$

Next, consider rotating  $\Phi_{n1}$  for  $\xi_{ni}$  and  $\Phi_{ni}$  for  $\xi_{ni} - \omega_{ni}$  around the  $Z$ -axis where:

$$\xi_{ni} = \tan^{-1} \frac{\sin \omega_{ni}}{(\cos \omega_{ni} - 1)} \quad (39)$$

Then,  $\Phi_{n1}$ ,  $\Phi_{ni}$ ,  $P_{n1}$ , and  $P_{ni}$  are transformed to  $\dot{\Phi}_{n1}$ ,  $\dot{\Phi}_{ni}$ ,  $\dot{P}_{n1}$ , and  $\dot{P}_{ni}$ :

$$\dot{P}_{n1} = \begin{bmatrix} \dot{X}_{n1} \\ \dot{Y}_{n1} \\ \dot{Z}_{n1} \end{bmatrix} = R_z(\xi_{ni}) \begin{bmatrix} X_{n1} + D_X \\ Y_{n1} \\ Z_{n1} \end{bmatrix} = \begin{bmatrix} (X_{n1} + D_X) \cos \xi_{ni} - Y_{n1} \sin \xi_{ni} \\ (X_{n1} + D_X) \sin \xi_{ni} + Y_{n1} \cos \xi_{ni} \\ Z_{n1} \end{bmatrix} \quad (40)$$

$$\dot{P}_{ni} = \begin{bmatrix} \dot{X}_{ni} \\ \dot{Y}_{ni} \\ \dot{Z}_{ni} \end{bmatrix} = R_Z(\xi_{ni} - \omega_{ni}) \begin{bmatrix} X_{n1} \cos \omega_{ni} - Y_{n1} \sin \omega_{ni} + D_X \\ X_{n1} \sin \omega_{ni} + Y_{n1} \cos \omega_{ni} \\ Z_{n1} \end{bmatrix} = \begin{bmatrix} (X_{n1} - D_X) \cos \xi_{ni} - Y_{n1} \sin \xi_{ni} \\ (X_{n1} - D_X) \sin \xi_{ni} - Y_{n1} \cos \xi_{ni} \\ Z_{n1} \end{bmatrix} \quad (41)$$

where  $\tan(\xi_{ni} - \omega_{ni}) = \sin \omega_{ni} / (1 - \cos \omega_{ni})$ . From Equations (40) and (41), the  $Y$ - and  $Z$ -coordinates of  $\dot{P}_{n1}$  and  $\dot{P}_{ni}$  are identical to one another. The perspective projections  $\dot{p}_{pn1}$  and  $\dot{p}_{pni}$  of  $\dot{P}_{pn1}$  and  $\dot{P}_{pni}$  can be computed also by rotating  $p_{pn1}$  for  $\xi_{ni}$  and  $p_{pni}$  for  $\xi_{ni} - \omega_{ni}$ :

$$\dot{p}_{pn1} = \begin{bmatrix} \dot{x}_{pn1} \\ \dot{y}_{pn1} \end{bmatrix} = R_{2D}(\xi_{ni}) p_{pn1} = \frac{f \cos \xi_{ni}}{Z_{n1}} \begin{bmatrix} X_{n1} - Y_{n1} \tan \xi_{ni} + D_X \\ X_{n1} \tan \xi_{ni} + Y_{n1} + D_X \tan \xi_{ni} \end{bmatrix} \quad (42)$$

$$\dot{p}_{pni} = \begin{bmatrix} \dot{x}_{pni} \\ \dot{y}_{pni} \end{bmatrix} = R_{2D}(\xi_{ni} - \omega_{ni}) p_{pni} = \frac{f \cos \xi_{ni}}{Z_{n1}} \begin{bmatrix} X_{n1} - Y_{n1} \tan \xi_{ni} + D_X \\ X_{n1} \tan \xi_{ni} + Y_{n1} + D_X \tan \xi_{ni} \end{bmatrix} \quad (43)$$

The  $y$ -coordinates of  $\dot{p}_{pn1}$  and  $\dot{p}_{oni}$  are also identical with one another and the distance between their  $x$ -coordinates depends on  $Z_{n1}$ . If  $\Phi_{n1}$  and  $\Phi_{ni}$  are individually planar,  $Z_{n1}$  becomes a function of  $X_{n1}$  and  $Y_{n1}$ . Then, both the  $x$ - and  $y$ -coordinates of  $\dot{p}_{pn1}$  and  $\dot{p}_{oni}$  become functions of  $X_{n1}$  and  $Y_{n1}$ . This introduces a systematic relation between perspective projections  $\dot{\phi}_{n1}$  and  $\dot{\phi}_{ni}$  of  $\dot{\Phi}_{n1}$  and  $\dot{\Phi}_{ni}$ .

Assume  $\dot{\Phi}_{n1}$  and  $\dot{\Phi}_{ni}$  are individually planar. Then, the following equation is satisfied by  $\dot{P}_{n1} = [\dot{X}_{n1} \ \dot{Y}_{n1} \ \dot{Z}_{n1}]^T$ :

$$a_{n1} \dot{X}_{n1} + b_{n1} \dot{Y}_{n1} + c_{n1} \dot{Z}_{n1} + d_{n1} = 0 \quad (44)$$

where  $a_{n1}$ ,  $b_{n1}$ ,  $c_{n1}$ , and  $d_{n1}$  are constants. From Equations (40), (41), and (44) (see Supplemental Materials):

$$\dot{x}_{n1} (2a_{n1} D_X \cos \xi_{ni} + d_{n1}) + 2\dot{y}_{n1} b_{n1} D_X \cos \xi_{ni} + 2f c_{n1} D_X \cos \xi_{ni} = d_{n1} \dot{x}_{ni} \quad (45)$$

Namely,  $x_{ni}$  can be represented as a weighted sum of  $x_{n1}$ ,  $y_{n1}$ , and a constant. From equations (42), (43), and (45), a relation between  $\dot{p}_{pn1}$  and  $\dot{p}_{oni}$  can be written as:

$$\dot{p}_{pni} = \begin{pmatrix} 2a_{n1}D_X \cos \xi_{ni}/d_{n1} + 1 & 2b_{n1}D_X \cos \xi_{ni}/d_{n1} \\ 0 & 1 \end{pmatrix} \dot{p}_{pn1} + f \begin{bmatrix} 2c_{n1}D_X \cos \xi_{ni}/d_{n1} \\ 0 \end{bmatrix} \quad (46)$$

Since  $\dot{p}_{pn1}$  and  $\dot{p}_{oni}$  are 2D rotations of  $p_{pn1}$  and  $p_{pni}$ , a relation between  $\varphi_{pn1}$  and  $\varphi_{pni}$  is:

$$R_{2D}(\xi_{ni} - \omega_{ni})p_{pni} = \begin{pmatrix} m_{11} & m_{12} \\ 0 & 1 \end{pmatrix} R_{2D}(\xi_{ni})p_{pn1} + f \begin{bmatrix} m_{13} \\ 0 \end{bmatrix} \quad (47)$$

where:

$$\begin{cases} m_{11} = 2a_{n1}D_X \cos \xi_{ni}/d_{n1} + 1 \\ m_{12} = 2b_{n1}D_X \cos \xi_{ni}/d_{n1} \\ m_{13} = 2c_{n1}D_X \cos \xi_{ni}/d_{n1} \end{cases}$$

Equation (46) shows that, after rotating  $\varphi_{pn1}$  for  $\xi_{ni}$  and  $\varphi_{pni}$  for  $\xi_{ni} - \omega_{ni}$ , a relation between these two curves in  $\Pi_I$  can be represented by a subgroup of the 2D affine transformation.

This is a combination of scaling, shear, and translation along the x-axis. It is worth pointing out that the same subgroup of the 2D affine transformation also appeared in Equations (25) and (34), which represent the relationship among orthographic projections of a 3D symmetrical set of planar curves.

QED

Note that  $\zeta_{ni} = 0$  and  $\xi_{ni} - \omega_{ni} = -\pi$  if  $i = n = 2$ . Then, the subgroup of the 2D affine transformation represents a relation between  $\varphi_{pn1}$  and the 180° rotation of  $\varphi_{pni}$  (see 3.2.3.2).

### 3.2.4.3. Model-based invariant under a 2D general perspective projection

**Theorem-B2.:** Let  $\Phi_{n1}, \Phi_{n2}, \dots, \Phi_{ni}, \dots, \Phi_{nn}$  be an  $n$ -fold 3D symmetrical set of planar curves and  $\varphi_{on1}, \varphi_{on2}, \dots, \varphi_{oni}, \dots, \varphi_{onn}$  be their perspective projections in a 2D image plane  $\Pi_I$  where  $i$  is a natural number between 1 and  $n$ . Assume that a perspective projection of their symmetry axis and a vanishing point  $v_{axis}$  of the axis in  $\Pi_I$  are given. Let us set the 2D  $xy$  Cartesian coordinate system on  $\Pi_I$  so that the origin is at the principal point and  $v_{axis}$  is on the  $x$ -axis:  $v_{axis} = [x_{axis} \ 0]^T$ . The projection of the symmetry axis can be written as  $v_{axis} + t[x_1 \ y_1]^T$  where  $t$  is a free parameter. Then, a relation between  $\varphi_{pn1}$  and  $\varphi_{pni}$  can be represented as follows:

$$\frac{R_Z(\xi_{ni} - \omega_{ni} - \sigma_a)R_Y^T(\sigma_v)}{x_{pni} \sin \sigma_v + f \cos \sigma_v} \begin{bmatrix} x_{pni} \\ y_{pni} \\ f \end{bmatrix} = \begin{pmatrix} m_{11} & m_{12} & m_{13} \\ 0 & 1 & 0 \\ 0 & 0 & 1 \end{pmatrix} \frac{R_Z(\xi_{ni} - \sigma_a)R_Y^T(\sigma_v)}{x_{pn1} \sin \sigma_v + f \cos \sigma_v} \begin{bmatrix} x_{pn1} \\ y_{pn1} \\ f \end{bmatrix} \quad (48)$$

$$\zeta_{ni} = \tan^{-1} \frac{\sin \omega_{ni}}{\cos \omega_{ni} - 1}$$

where  $p_{pn1} = [x_{pn1} \ y_{pn1}]^T$  and  $p_{pni} = [x_{pni} \ y_{pni}]^T$  are a pair of corresponding points on  $\varphi_{pn1}$  and  $\varphi_{pni}$ .  $f$  is a focal distance,  $\sigma_v = \text{atan}(x_{axis}/f)$ ,  $\sigma_a = \text{atan}(y_l/(x_l \cos \sigma_v))$ ,  $\omega_{ni} = 2\pi(i-1)/n$ , and  $m_{11}$ ,  $m_{12}$ , and  $m_{13}$  are free parameters.

**Proof:** In the prior sub-section, it was assumed that an axis of an  $n$ -fold 3D symmetrical set of planar curves is parallel to the  $Z$ -axis. We now consider the more general condition in which this assumption is not necessary. A camera of a perspective projection can be virtually rotated with the image plane  $\Pi_I$  and the 3D coordinate system around the center of projection arranged such that the assumption of the prior sub-section is satisfied. Note that the same procedure was used for the recovery of the 3D shape that was described in an earlier section of this study (see 3.2.2.2.).

Now, consider an  $n$ -fold 3D symmetrical set of planar curves ( $\Phi_{n1}, \Phi_{n2}, \dots, \Phi_{ni}, \dots, \Phi_{nn}$ ) and their perspective projections in the image plane  $\Pi_I$ . A projection  $I_{axis}$  of their symmetry axis and a vanishing point  $v_{axis}$  of the axis are given (see 3.1.1. and 3.2.1.1.). Set the orientation of the 2D  $xy$  Cartesian coordinate system so that  $v_{axis}$  is on the  $x$ -axis;  $v_{axis} = [x_{axis} \ 0]^T$ . The symmetry axis is parallel to a line connecting the center of projection  $F (= [0 \ 0 \ 0]^T)$  and  $[x_{axis} \ 0 \ f]^T$ . Any point on the projection of the symmetry axis can be written as  $v_{axis} + t[x_l \ y_l]^T$  where  $t$  is a free parameter.

The image is transformed by emulating a camera rotation  $R_v$  around the  $Y$ -axis so that the vanishing point is transformed to the principal point in the image plane  $\Pi_I$ .  $R_v = R_Y(\sigma_v)$  where  $\sigma_v = \text{atan}(x_{axis}/f)$ . Then, a point  $[x \ y]^T$  in the original image is transformed to  $[x' \ y']^T$  after  $R_v$  (see Supplemental Materials):

$$\begin{bmatrix} x' \\ y' \\ f \end{bmatrix} = \frac{f R_Y^T(\sigma_v)}{x \sin \sigma_v + f \cos \sigma_v} \begin{bmatrix} x \\ y \\ f \end{bmatrix} \quad (49)$$

A line connecting the center of projection  $F$  and the vanishing point ( $[0 \ 0]^T$ ) is parallel to the symmetry axis and is perpendicular to  $\Pi_I$  after  $R_v$ . The projection of the symmetry axis after  $R_v$  can be written as follows:

$$\frac{ft}{1 + tx_{axis} \sin \sigma_v} \begin{bmatrix} x_l \cos \sigma_v \\ y_l \end{bmatrix} \quad (50)$$

The projection of the symmetry axis becomes coincident with the  $x$ -axis after another camera rotation  $R_a (= R_Z(\sigma_a))$  around the  $Z$ -axis for  $\sigma_a = \text{atan}(y_l/(x_l \cos \sigma_v))$ :

$$R_Z^T(\sigma_a) \begin{bmatrix} x' \\ y' \\ f \end{bmatrix} = \frac{f R_Z^T(\sigma_a) R_Y^T(\sigma_v)}{x \sin \sigma_v + f \cos \sigma_v} \begin{bmatrix} x \\ y \\ f \end{bmatrix} \quad (51)$$

A transformation of the image caused by  $R_a$  is equivalent to a 2D image rotation:  $R_{2D}^T(\sigma_a)$ . After the camera rotation  $R_v R_a (= R_Y(\sigma_v) R_Z(\sigma_a))$ , the curves  $\Phi_{n1}, \Phi_{n2}, \dots, \Phi_{ni}, \dots, \Phi_{nn}$  satisfy all the conditions of the Lemma-for-Theorem-B2. Hence, from Equation (34) of Lemma-for-Theorem-B2, the relation between  $\varphi_{pn1}$  and  $\varphi_{pni}$  can be represented as follows:

$$\frac{R_Z(\xi_{ni} - \omega_{ni} - \sigma_a) R_Y^T(\sigma_v)}{x_{pni} \sin \sigma_v + f \cos \sigma_v} \begin{bmatrix} x_{pni} \\ y_{pni} \\ f \end{bmatrix} = \begin{pmatrix} m_{11} & m_{12} & m_{13} \\ 0 & 1 & 0 \\ 0 & 0 & 1 \end{pmatrix} \frac{R_Z(\xi_{ni} - \sigma_a) R_Y^T(\sigma_v)}{x_{pn1} \sin \sigma_v + f \cos \sigma_v} \begin{bmatrix} x_{pn1} \\ y_{pn1} \\ f \end{bmatrix} \quad (52)$$

where  $[x_{pn1} \ y_{pn1}]^T$  and  $[x_{pni} \ y_{pni}]^T$  are a pair of corresponding points on  $\varphi_{pn1}$  and  $\varphi_{pni}$  and  $m_{11}$ ,  $m_{12}$ , and  $m_{13}$  are free parameters.

QED

It is worth pointing out that the subgroup of the 2D affine transformation in Equation (52) also appears in a transformation representing the relationship between perspective projections of a 3D mirror-symmetrical pair of planar curves (Equation (20) in Sawada, Li, & Pizlo, 2014). But, Equation (52) has two rotation matrices  $R_Z(\xi_{ni} - \sigma_a)$  and  $R_Z(\xi_{ni} - \omega_{ni} - \sigma_a)$  that do not exist in the transformation used for 3D mirror-symmetry. Hence, Equation (52) is more complicated than the transformation for 3D mirror-symmetry.

#### 4. General Discussion

The study has shown that 3D rotational-symmetry has the following properties: (i) a 3D rotational-symmetrical shape can be recovered from one of its 2D images, (ii) any pair of 2D curves is consistent with a 3D, 2-fold rotational-symmetrical interpretation, and (iii) additional model-based invariants of 3D rotational-symmetry can be introduced under both orthographic and perspective projections if the 3D rotational-symmetrical set of curves are individually planar. Another important property of 3D rotational-symmetry is called a “virtual image” (Vetter & Poggio, 1994), namely, the single 2D image of the  $n$ -fold 3D symmetrical object is equivalent to  $n$  images of the same object seen from different viewpoints.

These properties are also present in 3D mirror-symmetry. Note, however, that it is computationally much harder to use 3D *rotational*-symmetry to recover a 3D shape than it is to use 3D *mirror*-symmetry to perform this kind of recovery. For example, the symmetry axis in 3D *rotational*-symmetry is specified by 4 parameters, 2 for orientation and 2 for position, but the symmetry plane in 3D *mirror*-symmetry can be specified by only 3 parameters, 2 for orientation and 1 for position (see 3.2.1.1.).<sup>8</sup> Note also that a 2D image of

a 3D rotationally-symmetrical pair of planar curves satisfy Equations (25), (34), or (48), depending on the type of projection. These equations represent the model-based invariants of the 3D *rotational*-symmetry, and the planarity of the curves. The model-based invariants of 3D *mirror*-symmetry and the planarity of the curves are also represented by analogous equations (Equations 1, 8, and 20 in Sawada, Li, & Pizlo, 2014) but, here again, the equations for 3D mirror-symmetry are simpler than those for 3D rotational symmetry. Also note that it is more difficult to find a corresponding pair of points in a 2D image of a 3D rotationally-symmetrical shape than in a 2D image of a 3D mirror-symmetrical shape. Consider two pairs of 2D curves in the image plane: one is an image of a 3D *rotational*-symmetrical pair of curves and the other is an image of a 3D *mirror*-symmetrical pair of curves. Each corresponding pair of points on the curves is established by finding intersections of the 2D curves with a *pair* of lines for 3D rotational-symmetry (see 3.2.3.) and with only a *single* line for 3D mirror-symmetry (Sawada, Li, & Pizlo, 2011; Rothwell, 1995; Hong, Ma, & Yu, 2004).

These complexities, which are inherent in using 3D rotational-symmetry compared with 3D mirror-symmetry, could actually be critical with respect to their utility within the human visual system. With 3D mirror-symmetry, a pair of curves in a 3D scene is easier to detect from its 2D image if the curves are individually planar (Sawada, Li, & Pizlo, 2011, 2014). This is not the case with 3D rotational-symmetry. We made some subjective observations that suggest that we can detect 3D rotational-symmetry only if the number of symmetry folds is sufficiently large (Figure 18). It also seems worthwhile to point out here that the boundary contour of a 2D image of a 3D rotationally symmetrical shape becomes closer to 2D mirror-symmetrical as the number of the folds increases. As the number of the folds increases, two regular features emerge in a 3D rotationally-symmetrical shape. First, a symmetry polygon of the 3D rotationally-symmetrical shape becomes closer to a circle, which is the most regular shape (Pizlo, 2008). A 2D image of the circle in the 3D scene is always an ellipse under both orthographic and perspective projections (Pizlo & Salach-Golyska, 1994). It is possible that the visual system is sensitive to the circle in the 3D scene (see Zanker & Quenzer, 1999) or the ellipse in the 2D image. The other emerging feature is 2D mirror-symmetry. A 3D rotationally-symmetrical shape becomes closer to a surface-of-revolution as the number of the folds increases, and the boundary contour of a 2D image of a surface-of-revolution is always 2D mirror-symmetrical under an orthographic projection (Figure 19) as well as under a perspective projection at least with the spherical retina of the "reduced" eye<sup>9</sup> (Horn & Brody, 1988). The visual system is very sensitive to 2D mirror-symmetry in a retinal image (e.g. Barlow & Reeves, 1979; Jenkins, 1983; Cohen & Zaidi, 2013). All of these observations suggest that the human visual system is relatively insensitive to 3D rotational-symmetry, at least when the number of the folds in the shape is small.

<sup>8</sup>There is no difference between 2D rotational- and mirror-symmetry in this aspect. Both the symmetry point of 2D rotational-symmetry and the symmetry axis of 2D mirror-symmetry can be specified by 2 parameters.

<sup>9</sup>If the image is planar under a perspective projection, the boundary contour can be represented by a Kanatani transformation (Kanatani, 1988) of a 2D mirror-symmetrical shape whose axis passes the principal point (Wong, Mendonça, & Cipolla, 2004).

On the other hand, the virtual image of a 3D rotational-symmetrical object is computationally easier to generate than the virtual image of a 3D mirror-symmetrical object with a single symmetry plane. Virtual images of the same objects from different viewpoints can be generated from images of these symmetrical objects (Vetter & Poggio, 1994). The virtual image of a rotational-symmetrical object is identical to the original image, but the virtual image of a mirror symmetrical object is identical to the “reflection” of the original image. The virtual image of a mirror symmetrical object is computationally more complex because of this reflection. Consider the human’s recognition of the 3D shape of an object. Human performance in 3D shape recognition tasks is reliable with a 3D mirror-symmetrical object that has a single symmetry plane, but not with a 3D asymmetrical object (Li & Pizlo, 2011; Chan, Stevenson, Li, & Pizlo, 2006; Liu, Knill, & Kersten, 1995; Liu & Kersten, 2003; Pizlo & Stevenson, 1999; van Lier & Wagemans, 1999; Vetter, Poggio, & Bühlhoff, 1994). This superior performance with the mirror-symmetrical object could be explained by a mechanism based only on the 2D template matching of memorized images of the object, or on a 2D image interpolation between the memorized images (e.g. Bühlhoff, Edelman, & Tarr, 1995). The virtual image of the mirror-symmetrical object could serve as an additional memorized image for an image-based mechanism. If this applied here, human performance when recognizing a rotational symmetrical object should be better than performance when recognizing a mirror-symmetrical object. Note that the virtual image of the rotational-symmetrical object is more easily generated than the virtual image of the mirror-symmetrical object. We know of no psychophysical study that tested recognition with a 3D rotational-symmetrical object, but based on our subjective observations, it is easy to see that it is difficult to recognize 3D rotational-symmetrical objects from different views when they only have a small number of symmetry folds (see Figure 18).

The human visual system can detect the 3D rotational-symmetry of an object reliably from its 2D image only under limited conditions, for example, when there are many symmetry folds (Figure 18), or when the object is close to being flat (Figure 1D), and when the object is viewed from a degenerate viewpoint that makes its 2D retinal image rotational-symmetrical (e.g. a right-bottom flower in Figure 1A). Another possible condition is when the shape of the object (or parts composing the object, see Figure 17) satisfies some other important constraints for recovering the veridical 3D shape of the object from a 2D image. Under this condition, the human visual system can detect the 3D rotational-symmetry of the object, but not from the image itself. It can detect it from the 3D shape perceived from the 2D image. For example, the 3D shape of an object is perceived reliably if the object is 3D mirror-symmetrical (Li et al., 2009, 2011; Pizlo et al., 2010, 2014). This detection is rather common. Some 3D rotational-symmetrical objects in real life are also 3D mirror-symmetrical (see Figure 1DF for examples). Also, any 3D mirror-symmetrical object with multiple symmetry planes is always 3D rotational-symmetrical (Stewart & Golubitsky, 1992; van der Helm & Leeuwenberg, 1996, see Figure 20 for illustration of this relation between rotational- and mirror symmetry using 2D figures). On the other hand, a 3D rotational-symmetrical object with multiple folds is not necessarily 3D mirror-symmetrical (see Figure 1ABC for examples).

In this study, we studied the geometrical properties of 3D rotational-symmetry, specifically, the 3D shape of a 3D rotational-symmetrical object and its 2D projection. Interestingly, 3D

rotational-symmetry shares many geometrical properties with 3D mirror-symmetry, but based on our subjective observations, these two types of symmetry seem to be perceived in very different ways. We plan to study these perceptual differences in psychophysical experiments in our future work.

## Supplementary Material

Refer to Web version on PubMed Central for supplementary material.

## Acknowledgement

This project was supported by National Eye Institute Grants EY013312 to Q. Zaidi.

## References

- Barlow HB, & Reeves BC (1979). The versatility and absolute efficiency of detecting mirror symmetry in random dot displays. *Vision Research*, 19, 783–793. [PubMed: 483597]
- Biederman I (1987). Recognition-by-components: A theory of human image understanding. *Psychological Review*, 94, 115–147. [PubMed: 3575582]
- Biederman I & Gerhardstein PC (1993). Recognizing depth-rotated objects: Evidence and conditions for three-dimensional viewpoint invariance. *Journal of Experimental Psychology: Human Perception and Performance*, 19, 1162–1182 [PubMed: 8294886]
- Binford T (1971). Visual perception by computer. *IEEE Conference on Systems and control*, Vol. 261, p. 262.
- Bingham GP & Muchisky MM (1993a). Center of mass perception and inertial frames of reference. *Perception & Psychophysics*, 54, 617–632. [PubMed: 8290330]
- Bingham GP & Muchisky MM (1993b). Center of mass perception: Perturbation of symmetry. *Perception & Psychophysics*, 54, 633–639. [PubMed: 8290331]
- Bülthoff HH, Edelman SY, & Tarr MJ (1995). How are three-dimensional objects represented in the brain? *Cerebral Cortex*, 5, 247–260 [PubMed: 7613080]
- Chan MW, Stevenson AK, Li Y, & Pizlo Z (2006). Binocular shape constancy from novel views: The role of a priori constraints. *Perception & Psychophysics*, 68, 1124–1139. [PubMed: 17355037]
- Clarke ADF, Green PR, Halley F, & Chantler MJ (2011). Similar symmetries: The role of wallpaper groups in perceptual texture similarity. *Symmetry*, 3, 246–264.
- Cohen EH & Zaidi Q (2013). Symmetry in context: Salience of mirror symmetry in natural patterns. *Journal of Vision*, 13(6): 22.
- Culbert BM & Forrest JRK (2016). Floral symmetry affects bumblebee approach consistency in artificial flowers. *Journal of Pollination Ecology*, 18, 1–6.
- Fischler MA & Bolles RC (1981). Random sample consensus: A paradigm for model fitting with applications to image analysis and automated cartography. *Communications of the ACM*, 24, 381–395.
- Gao X, Hou X, Tang J, Cheng H (2003). Complete solution classification for the perspective three-point problem. *IEEE Transactions on Pattern Analysis and Machine Intelligence*, 25, 930–943
- Garner WR & Clement DE (1963). Goodness of pattern and pattern uncertainty. *Journal of Verbal Learning and Verbal Behavior*, 2, 446–452
- Gordon G (1990). Shape from symmetry. In *Proceedings of the Intelligent Robots and Computer Vision VIII: Algorithms and Techniques*, vol. 1192 (pp. 297–308).
- Hamada J & Ishihara T (1988). Complexity and goodness of dot patterns varying in symmetry. *Psychological Research*, 50, 155–161. [PubMed: 3217473]
- Hamada J Amano K, Fukuda ST, Fukushi K, & van der Helm PA (2016). A group theoretical model of symmetry cognition. *Acta Psychologica*, 171, 128–137 [PubMed: 27974278]

- Hargittal M & Hargittal I (1997). Symmetry perception: Logos of rotational-point-groups induce the feeling of motion. *Mathematical Intelligencer*, 19, 55–58.
- Hartley R & Zisserman A (2003). *Multiple View Geometry in Computer Vision* Cambridge, MA: Cambridge University Press.
- Hershenson M & Ryder J (1982). Perceived symmetry and visual matching. *American Journal of Psychology*, 95, 669–680 [PubMed: 7168458]
- Hilbert D, & Cohn-Vossen S (1952). *Geometry and the imagination* New York, NY: Chelsea.
- Hong W, Ma Y, & Yu Y (2004). Reconstruction of 3-D deformed symmetric curves from perspective images without discrete features In Pajdla T & Matas J (Eds.), *Computer Vision-ECCV 2004: ser. Lecture Notes in Computer Science*, vol. 3023 (pp. 533–545). Berlin, Germany: Springer-Verlag.
- Hong W, Yang AY, Huang K, & Ma Y (2004). On symmetry and multiple-view geometry: structure, pose, and calibration from a single image. *International Journal of Computer Vision*, 60,241–265.
- Horaud R and Brady M (1988). On the geometric interpretation of image contours. *Artificial Intelligence*, 37, 333–353.
- Jenkins B (1983). Component processes in the perception of bilaterally symmetric dot textures. *Perception & Psychophysics*, 34, 433–440. [PubMed: 6657447]
- Julesz B (1971). *Foundation of cyclopean perception* Chicago: University of Chicago Press.
- Kahn JI & Foster DH (1986). Horizontal-vertical structure in the visual comparison of rigidly transformed patterns. *Journal of Experimental Psychology: Human Perception and Performance*, 12, 422–433. [PubMed: 2946799]
- Kanade T (1981). Recovery of the three-dimensional shape of an object from a single view. *Artificial Intelligence*, 17, 409–460
- Kanade T, & Kender JR (1983). Mapping image properties into shape constraints: Skewed symmetry, affine-transformable patterns, and the shape-from-texture paradigm. In Beck J, Hope B,& Rosenfeld A (Eds.), *Human and machine vision* (pp. 237–257). New York: Academic Press.
- Kanatani K (1988). Constraints on length and angle. *Computer Vision, Graphics, and Image Processing*, 41, 28–42.
- Kohler PJ, Clarke A, Yakovleva A, Liu Y, & Norcia AM (2016). Representation of maximally regular textures in human visual cortex. *Journal of Neuroscience*, 36, 714–729. [PubMed: 26791203]
- Latecki LJ, Rosenfeld A (1998). Supportedness and tameness: Differentialless geometry of plane curves. *Pattern Recognition*, 31, 607–622.
- Li Y, Pizlo Z, & Steinman RM (2009). A computational model that recovers the 3D shape of an object from a single 2D retinal representation. *Vision Research*, 49, 979–91. [PubMed: 18621410]
- Li Y & Pizlo Z (2011). Depth cues vs. simplicity principle in 3D shape perception. *Topics in Cognitive Science*, 3, 667–685. [PubMed: 25164504]
- Li Y, Sawada T, Shi Y, Kwon T, & Pizlo Z (2011). A Bayesian model of binocular perception of 3D mirror symmetrical polyhedra. *Journal of Vision*, 11(4):11, 1–20.
- Li Y, Sawada T, Latecki LM, Steinman RM, & Pizlo Z (2012). A tutorial explaining a machine vision model that emulates human performance when it recovers natural 3D scenes from 2D images. *Journal of Mathematical Psychology*, 56(4), 217–231.
- Liu Y, Collins RT, & Tsin Y (2004). A computational model for periodic pattern perception based on frieze and wallpaper groups. *IEEE Transactions on Pattern Analysis and Machine Intelligence*, 26, 354–371. [PubMed: 15376882]
- Liu Z, & Kersten D (2003). Three-dimensional symmetric shapes are discriminated more efficiently than asymmetric ones. *Journal of the Optical Society of America A, Optics, Image Science, and Vision*,20, 1331–1340.
- Liu Z, Knill DC, & Kersten D (1995). Object classification for human and ideal observers. *Vision Research*, 35, 549–568. [PubMed: 7900295]
- Mach E (1906/1959). *The analysis of sensations and the relation of the physical to the psychical* New York: Dover.
- Makin ADJ, Pecchinenda A, & Bertamini M (2012). Implicit affective evaluation of visual symmetry. *Emotion*, 12, 1021–1030. [PubMed: 22251051]

- Makin ADJ, Rampone G, Pecchinenda A, & Bertamini M (2013). Electrophysiological responses to visuospatial regularity. *Psychophysiology*, 50, 1045–1055. [PubMed: 23941638]
- Makin ADJ, Wilton MM, Pecchinenda A, & Bertamini M (2012). Symmetry perception and affective responses: A combined EEG/EMG study. *Neuropsychologia*, 50, 3250–3261. [PubMed: 23063934]
- Metzger W (2009). *Laws of seeing* translated by L Spillman & S Lehar Cambridge: MIT Press (Originally published as: Metzger, W. 1936. *Gesetze des Sehens*. Kramer, Frankfurt.)
- Michaux A, Kumar V, Jayadevan V, Delp E, & Pizlo Z (2017). Binocular 3D object recovery using a symmetry prior. *Symmetry*, 9(5), 64.
- Minkov V, & Sawada T (2018). Seeing a Triangle in a 3D Scene Monocularly and Binocularly. NRU Higher School of Economics Series PSY “Psychology”, WP BRP 91/PSY/2018. Retrieved from [https://wp.hse.ru/en/prepfr\\_Psychology](https://wp.hse.ru/en/prepfr_Psychology)
- Mitsumoto H, Tamura S, Okazaki K, Kajimi N, & Fukui Y (1992). 3-D reconstruction using mirror images based on a plane symmetry recovering method. *IEEE Transactions on Pattern Analysis and Machine Intelligence*, 14, 941–946.
- Møller AP & Thornhill R (1998). Bilateral symmetry and sexual selection: A meta-analysis. *American Naturalist*, 151, 174–192.
- Møller AP, Thornhill R, & Gangestad SW (2005). Direct and indirect tests for publication bias: Asymmetry and sexual selection. *Animal Behavior*, 70, 497–506.
- Neal PR, Dafni A, & Giurfa M (1998). Floral symmetry and its role in plant-pollinator systems: Terminology, distribution, and hypotheses. *Annual Review of Ecology and Systematics*, 29, 345–373.
- Palmer SE (1991). Goodness, Gestalt, groups, and Garner: Local symmetry subgroups as a theory 1140 of figural goodness. In Lockhead GR & Pomerantz JR (Eds.), *The perception of structure: Essays in honor of Wendell R. Garner* (pp. 23–39). Washington, DC: American Psychological Association
- Palmer SE & Hemenway K (1978). Orientation and symmetry: Effects of multiple, rotational, and new symmetries. *Journal of Experimental Psychology: Human Perception and Performance*, 4, 691–702. [PubMed: 722256]
- Pentland AP (1986). Perceptual organization and the representation of natural form. *Artificial Intelligence*, 28, 293–331.
- Pizlo Z (2008). *3D shape: Its unique place in visual perception* Cambridge, MA: MIT Press.
- Pizlo Z, Li Y, Sawada T & Steinman RM (2014). *Making a Machine That Sees Like Us* New York, NY: Oxford University Press.
- Pizlo Z & Salach-Golyska M (1994). Is vision metric? Comment on Lappin and Love (1992). *Perception & Psychophysics*, 55, 230–234 [PubMed: 8036104]
- Pizlo Z, Sawada T, Li Y, Kropatsch W, & Steinman RM (2010). New Approach to the Perception of 3D Shape Based on Veridicality, Complexity, Symmetry and Volume. *Vision Research*, 50, 1–11. [PubMed: 19800910]
- Pizlo Z, & Stevenson AK (1999). Shape constancy from novel views. *Perception & Psychophysics*, 61, 1299–1307 [PubMed: 10572459]
- Rothwell CA (1995). *Object recognition through invariant indexing* Oxford, England: Oxford University Press.
- Royer FL (1981). Detection of symmetry. *Journal of Experimental Psychology: Human Perception and Performance*, 7, 1186–1210. [PubMed: 6458647]
- Saunders JA, & Knill DC (2001). Perception of 3D surface orientation from skew symmetry. *Vision Research*, 41, 3163–3183. [PubMed: 11711141]
- Savriama Y & Klingenberg CP (2011). Beyond bilateral symmetry: Geometric morphometric methods for any type of symmetry. *BMC Evolutionary Biology*, 11:280. [PubMed: 21958045]
- Sawada T, & Pizlo Z (2008). Detection of skewed symmetry. *Journal of Vision*, 8(5):14, 1–18
- Sawada T (2010). Visual detection of symmetry of 3D shapes. *Journal of Vision*, 10(6):4, 1–22.
- Sawada T, Li Y, & Pizlo Z (2011). Any pair of 2D curves is consistent with a 3D symmetric interpretation. *Symmetry*, 3, 365–388.

- Sawada T, Li Y, & Pizlo Z (2014). Detecting 3-D Mirror Symmetry in a 2-D Camera Image for 3-D Shape Recovery. *Proceedings of the IEEE*, 102, 1588–1606.
- Sawada T, Li Y, & Pizlo Z (2015). Shape Perception. In Busemeyer J, Townsend J, Wang ZJ, & Eidels A (Eds.), *Oxford Handbook of Computational and Mathematical Psychology* (pp. 255–276). New York, NY: Oxford University Press
- Stewart I & Golubitsky M (1992/1993). *Fearful Symmetry: Is God a Geometer?* London, UK: Penguin books.
- Sugihara K (2016). Anomalous Mirror Symmetry Generated by Optical Illusion. *Symmetry*, 8(4), 21.
- Swaddle JP (1999). Visual signaling by asymmetry: A review of perceptual processes. *Philosophical Transactions: Biological Sciences*, 354, 1383–1393. [PubMed: 10515000]
- Szlyk JP, Rock I, & Fisher CB (1995). Level of processing in the perception of symmetrical forms viewed from different angles. *Spatial Vision*, 9, 139–150. [PubMed: 7626544]
- Szlyk JP, Seiple W & Xie W (1995). Symmetry discrimination in patients with retinitis pigmentosa. *Vision Research*, 35, 1633–1640. [PubMed: 7667920]
- van der Helm PA & Leeuwenberg ELJ (1996). Goodness of visual regularities: A nontransformational approach. *Psychological Review*, 103, 429–456. [PubMed: 8759043]
- van der Vloed G, Csathó A, & van der Helm PA (2005). Symmetry and repetition in perspective. *Acta Psychologica*, 120, 74–92. [PubMed: 15932747]
- Van Gool L, Moons T, & Proesmans M (1996). Mirror and point symmetry under perspective skewing. In *Proceedings CVPR IEEE Computer Society Conference on Computer Vision and Pattern Recognition* (pp. 285–292), 10.1109/CVPR.1996.517087.
- van Lier R & Wagemans J (1999). From images to objects: Global and local completions of self-occluded parts. *Journal of Experimental Psychology: Human Perception and Performance*, 25, 1721–1741.
- Varley J, DeChant C, Richardson A, Ruales J, & Allen P (2017). Shape completion enabled robotic grasping. *IEEE/RSJ International Conference on Intelligent Robots and Systems (IROS)*. 2442–2447.
- Vetter T, & Poggio T (1994). Symmetric 3D objects are an easy case for 2D object recognition. *Spatial Vision*, 8, 443–453 [PubMed: 7772550]
- Vetter T, Poggio T, & Bühlhoff HH (1994). The importance of symmetry and virtual views in 1198 three-dimensional object recognition. *Current Biology*, 4, 18–23. [PubMed: 7922306]
- Wagemans J (1992). Perceptual use of nonaccidental properties. *Canadian Journal of Psychology*, 46, 236–279. [PubMed: 1451043]
- Wagemans J (1993). Skewed symmetry: A nonaccidental property used to perceive visual forms. *Journal of Experimental Psychology: Human Perception and Performance*, 19, 364–380. [PubMed: 8473845]
- Wagemans J (1995). Detection of visual symmetries. *Spatial Vision*, 9, 9–32 [PubMed: 7626549]
- Wagemans J (1997). Characteristics and models of human symmetry detection. *Trends in Cognitive Sciences*, 1, 346–352. [PubMed: 21223945]
- Wagemans J, Van Gool L, Swinnen V, & Van Horebeek J (1993). Higher-order structure in regularity detection. *Vision Research*, 33, 1067–1088. [PubMed: 8506646]
- Westphal-Fitch G, Huber L, Gómez JC, & Fitch WT (2012). Production and perception rules underlying visual patterns: Effects of symmetry and hierarchy. *Philosophical Transactions of the Royal Society B*, 367, 2007–2022.
- Weyl H (1952). *Symmetry* Princeton, NJ: Princeton University Press.
- Wong KK, Mendonça PRS, & Cipolla R (2004). Reconstruction of surfaces of revolution from single uncalibrated views. *Image and Vision Computing*, 22, 829–836.
- Yang AY, Huang K, Rao S, Hong W, & Ma Y (2005). Symmetry-based 3-D reconstruction from perspective images. *Computer Vision and Image Understanding*, 99, 210–240.
- Zanker JM & Quenzer T (1999). How to tell circles from ellipses: Perceiving the regularity of simple shapes. *Naturwissenschaften*, 86, 492–495. [PubMed: 10541660]

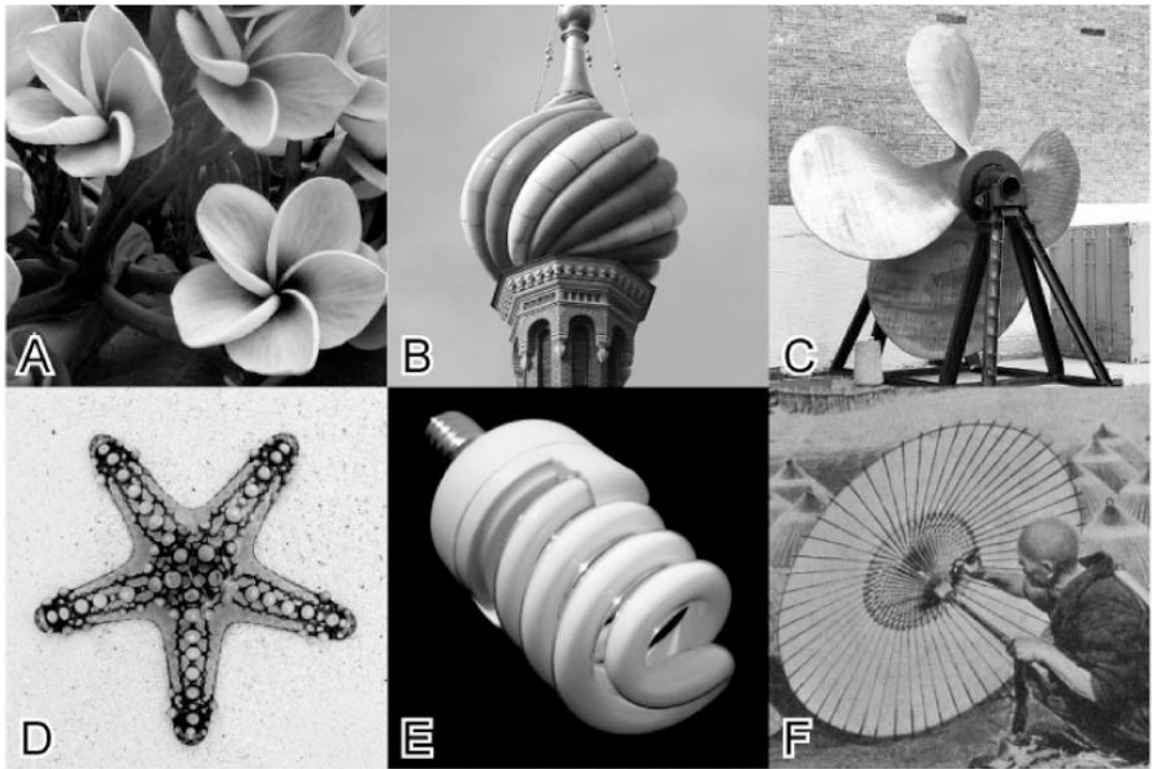


**Figure 1.**  
Rotational-symmetrical objects in real life.

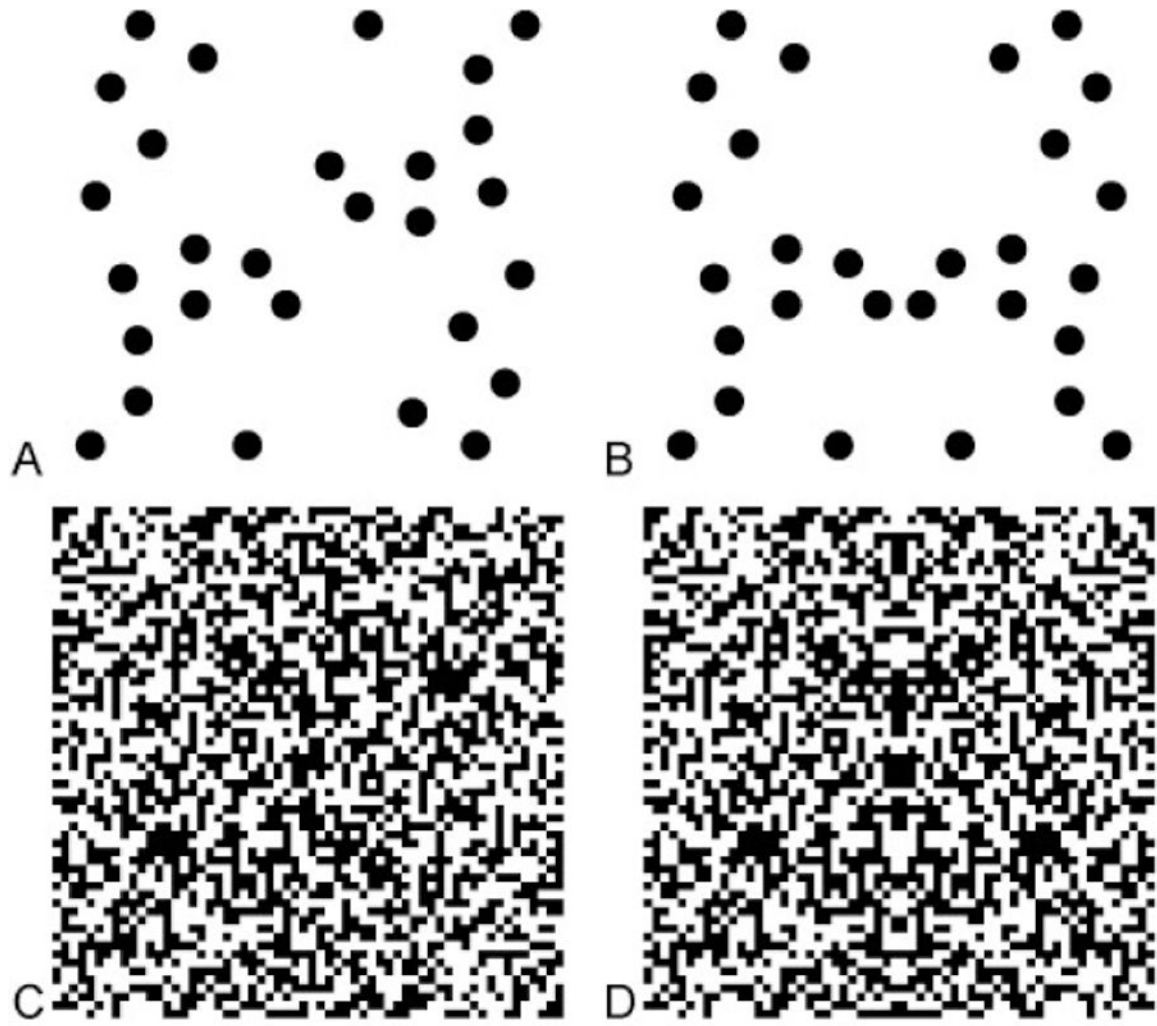


**Figure 2.** Random-dot patterns with (A, C) rotational- and (B, D) mirror-symmetry with two different densities.

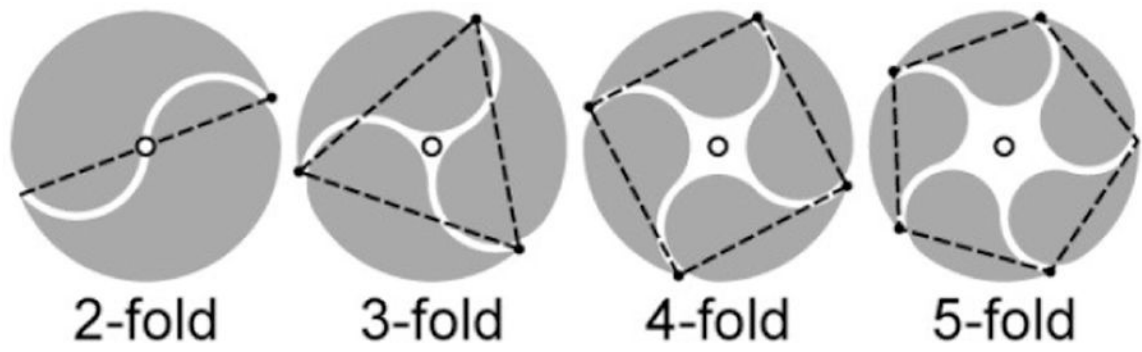


**Figure 3.**

2D symmetrical figures with 2-, 3-, 4-, and 5-folds. Their symmetry points are indicated by open circles and their symmetry polygons are drawn with dashed lines.

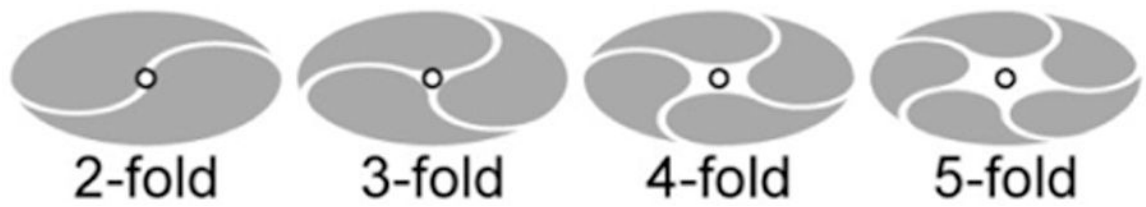


**Figure 4.** Orthographic projections of planar symmetrical figures in Figure 3 from viewing directions slanted  $60^\circ$  from their symmetry axes. Projections of their symmetry points are indicated by open circles. Note that the orthographic projections of the 2- and 4-fold symmetrical figures are also 2-fold symmetrical.

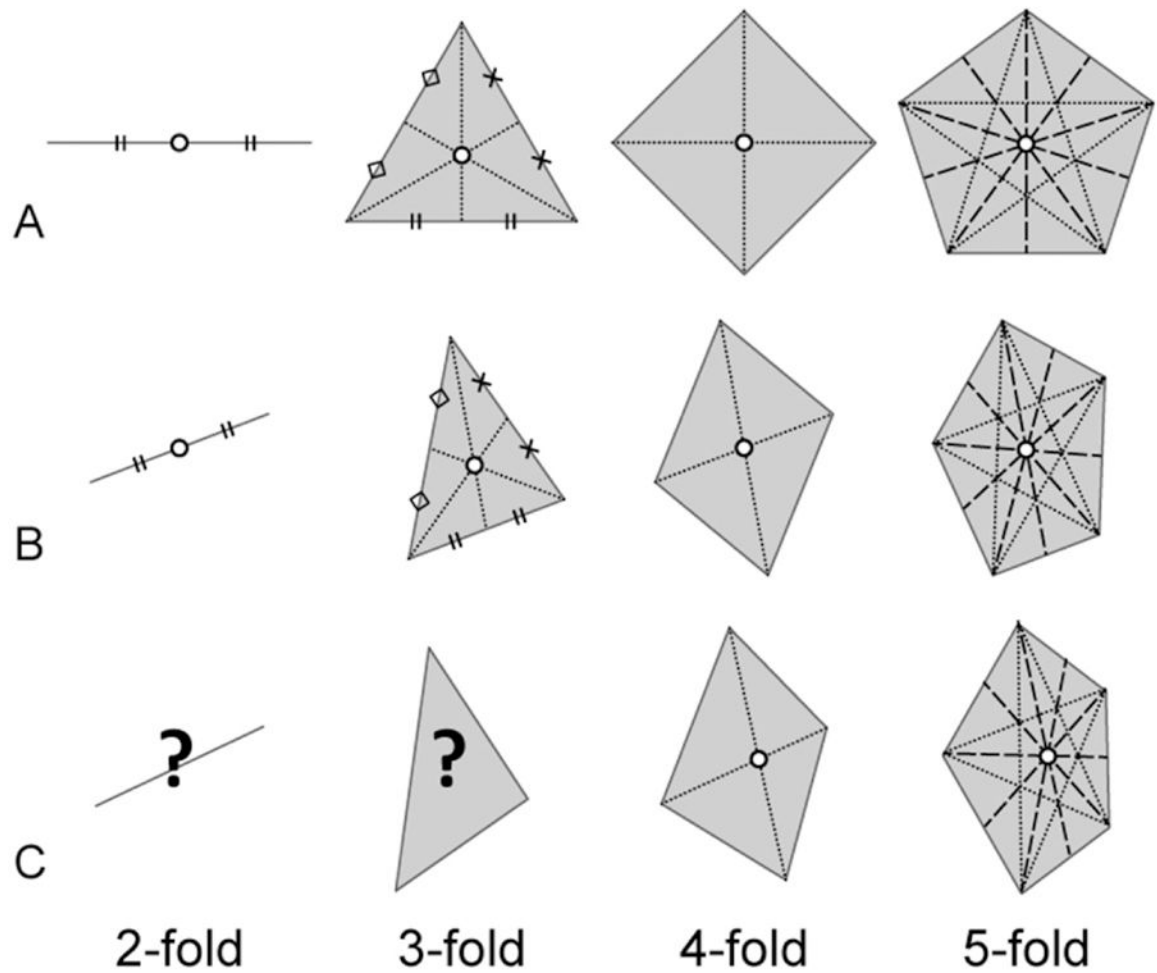


**Figure 5.**

(A) Symmetry polygons with 2-, 3-, 4-, 5-folds and their (B) orthographic and (C) perspective projections. The perspective projections of the symmetry points (open circles) can be derived from the perspective projections of the symmetry polygons only if the number of the folds is more than three. Auxiliary lines for finding the symmetry points are rendered in dotted and dashed lines. The projections of the symmetry points cannot be derived from the 2- or 3-fold symmetry polygons alone.

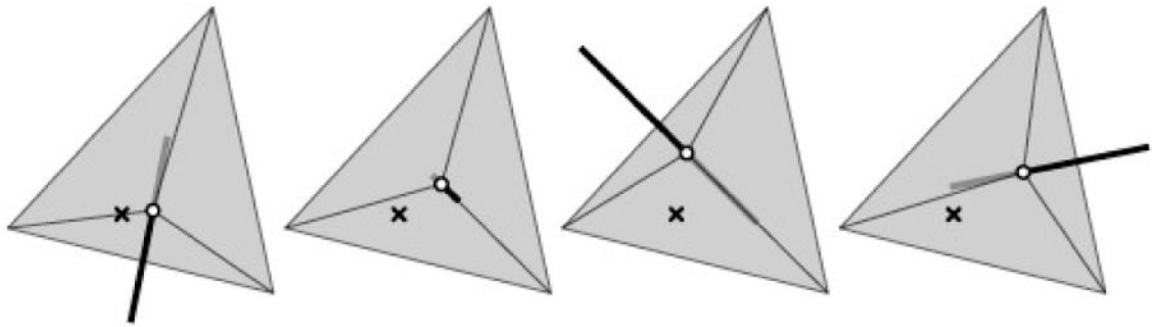


**Figure 6.** Perspective projections of a 3-fold symmetry polygon (equilateral triangle) with its symmetry axis with four different orientations. The four images of the symmetry polygon are identical to one another. The Principal points of the perspective projection are indicated by 'x'.

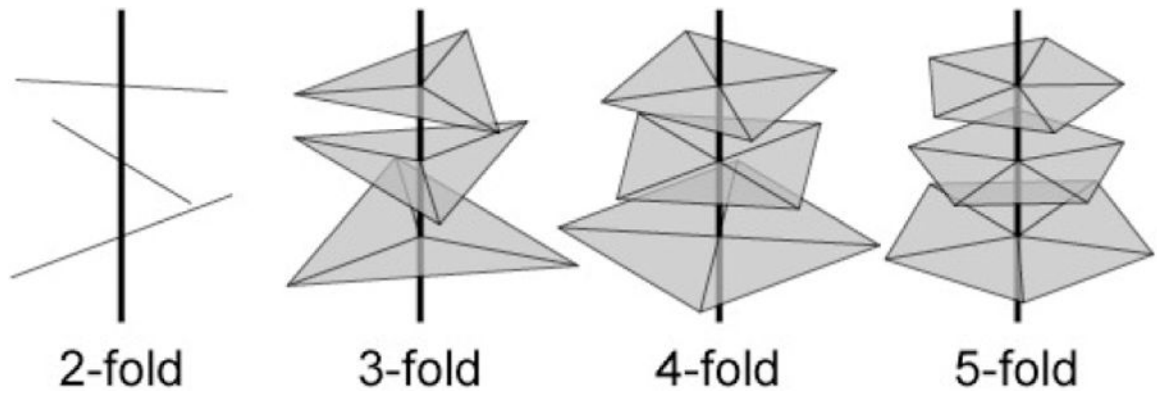


**Figure 7.** Orthographic projections of 3D symmetrical objects with 2-, 3-, 4-, and 5-folds. Their symmetry axes are indicated by thick line segments and symmetry polygons are drawn in gray.

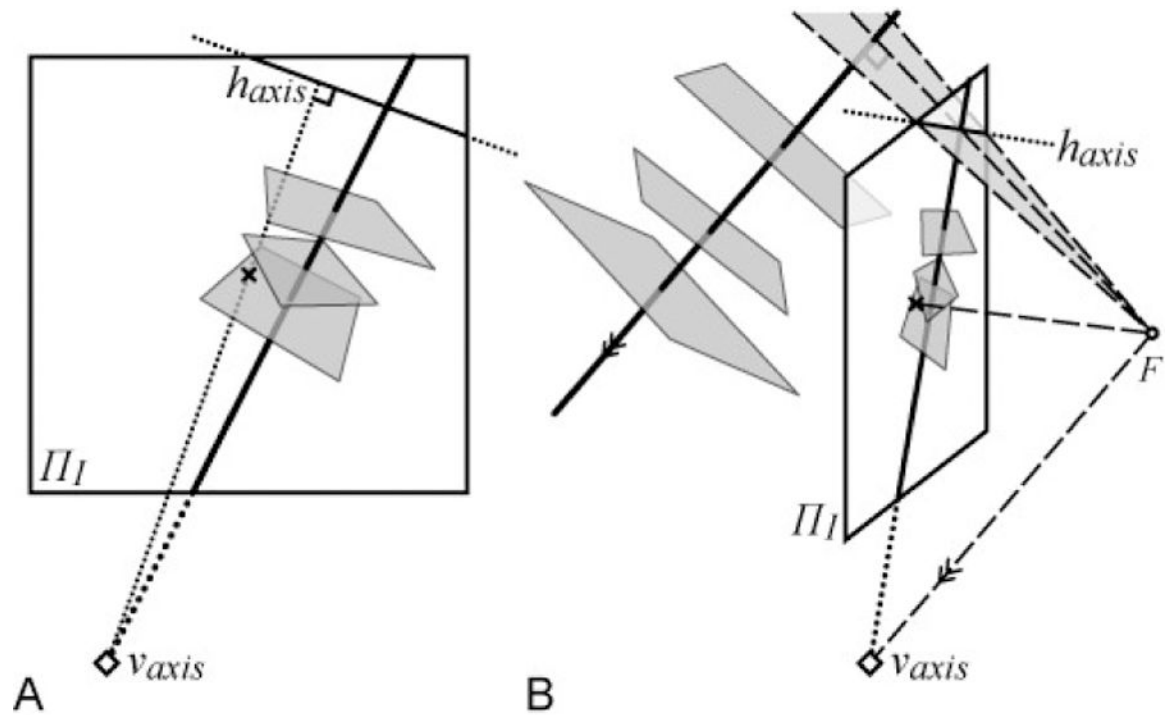


**Figure 8.**

A perspective projection of a 4-fold symmetrical object to the image plane  $\Pi_f$ . The symmetry axis is parallel to a line connecting the vanishing point  $v_{axis}$  of the symmetry axis and the center of projection  $F$ . A plane including  $F$  and the horizon  $h_{axis}$  of the symmetry axis is normal to the symmetry axis and to the segment  $Fv_{axis}$  and are parallel to the symmetry polygons.

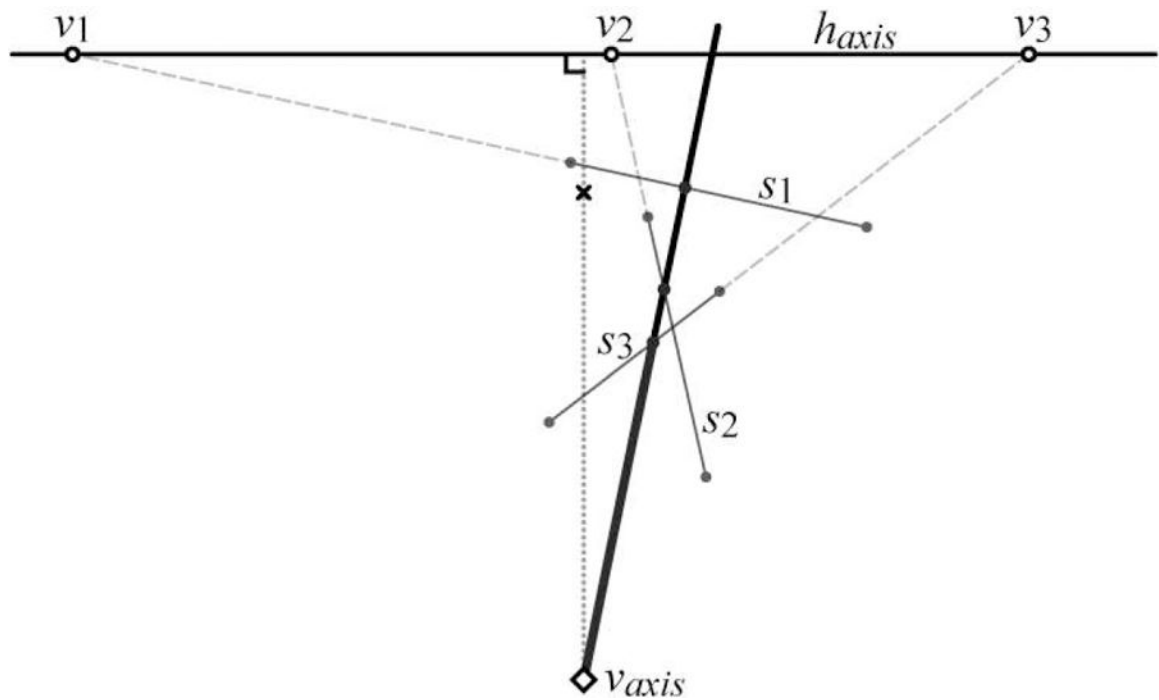


**Figure 9.**

A perspective projection of a 2-fold symmetrical object. The vanishing points  $v_1$ ,  $v_2$ , and  $v_3$  of the symmetry polygons are collinear on the horizon  $h_{axis}$  of the symmetry axis.

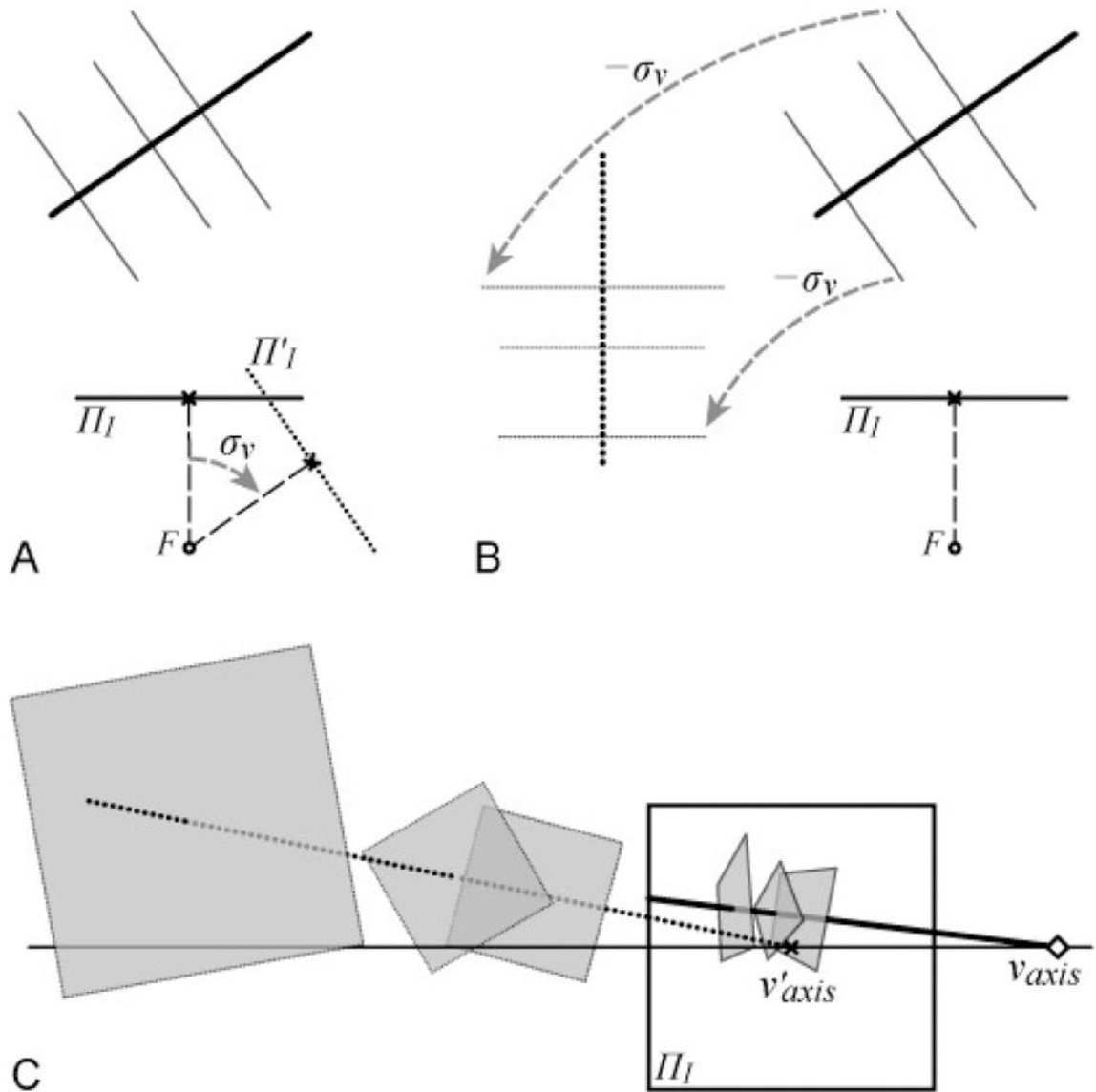


**Figure 10.**

(A) A perspective projection and another projection after rotating the camera (the principal axis and the image plane  $\Pi_I$ ) for  $\sigma_v$  about the center of projection  $F$  so that the symmetry axis becomes normal to  $\Pi'_I$ . (C) The original perspective image (solid) and the image after the rotation (dotted). The image after the rotation can be computed directly by transforming the original 2D image. (B) The transformation of the image by rotating the camera is the same as the image transformation by rotating the 3D scene about  $F$  in the opposite direction.

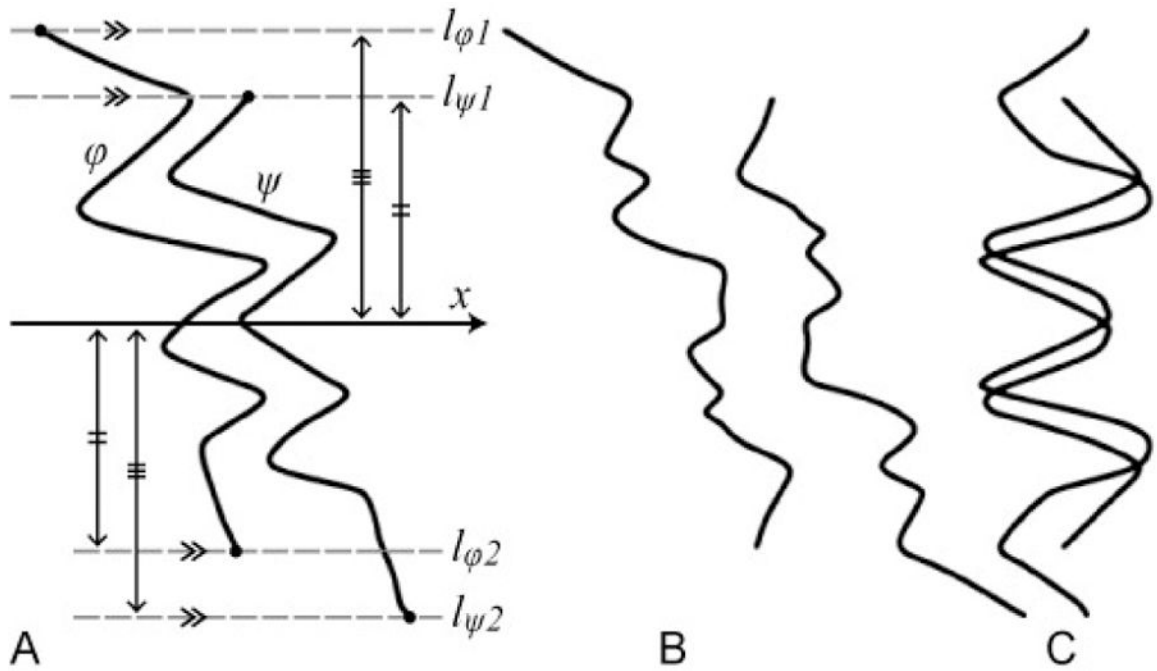


**Figure 11.**

(A) A pair of 2D curves  $\phi$  and  $\psi$  satisfying conditions of Theorem-A1 and (B, C) two views of their 3D symmetrical interpretation. The symmetrical interpretation was constructed by assuming that the slant of its symmetry axis is  $45^\circ$  under an orthographic projection. (B, C) Two orthographic images of the interpretation with its symmetry axis normal to the image plane (B) and with the symmetry axis parallel to the image plane (C). Note that the image in (B) is 2D rotational symmetrical and that in (C) is 2D mirror-symmetrical. These are properties 3D rotational-symmetry under the 2D orthographic projection. See Demo 1 in supplemental material for an interactive illustration of the 3D symmetric curves (the demo is also available at: <http://tadamasawada.com/demos/rotsym/>).

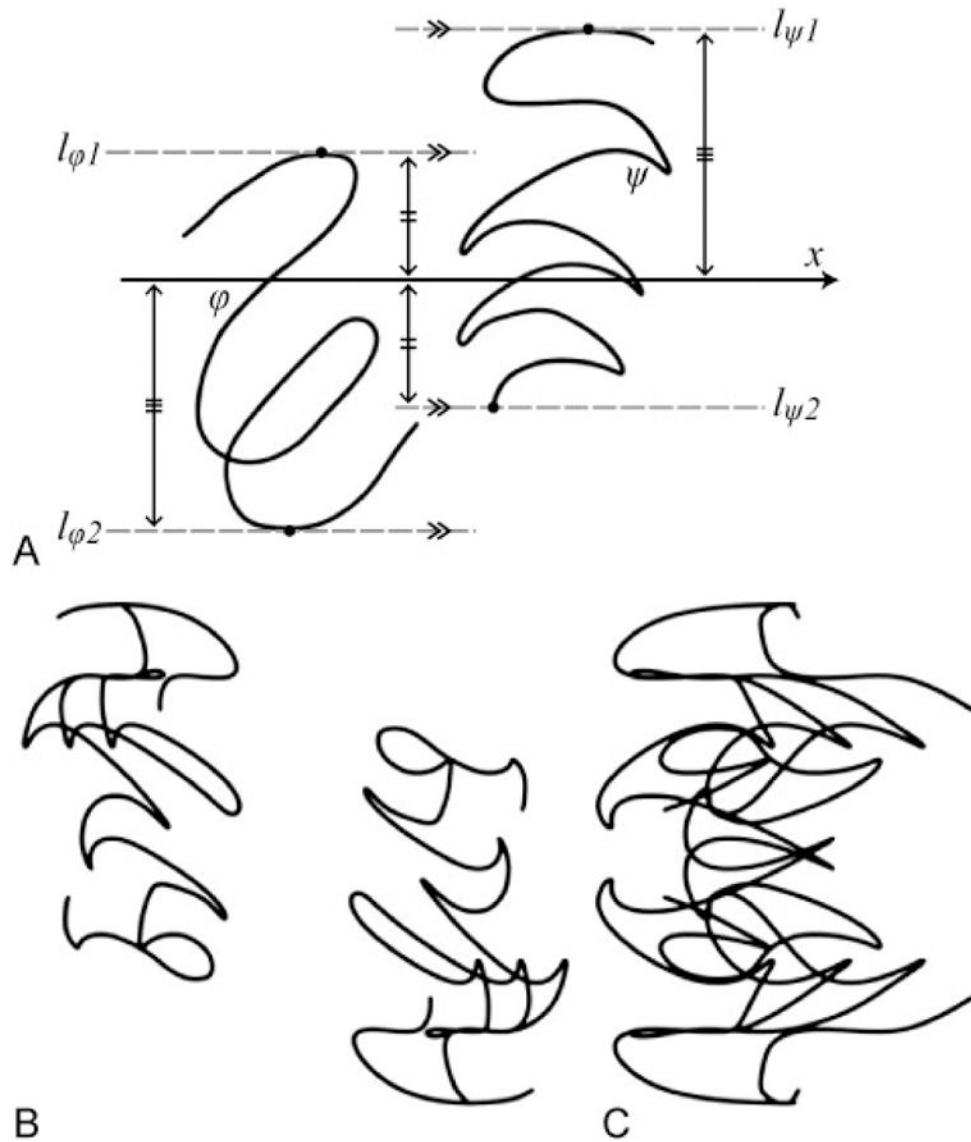


**Figure 12.**

(A) A pair of 2D curves  $\varphi$  and  $\psi$  satisfying conditions of Theorem-A1 and (B, C) two views of their 3D symmetrical interpretation. Some point on one curve in (A) corresponds with multiple points on the other curve and vice versa for the 3D rotational-symmetrical interpretation. The symmetrical interpretation was constructed by assuming that the slant of its symmetry axis is  $30^\circ$  under an orthographic projection. (B, C) Two orthographic images of the interpretation with its symmetry axis normal to the image plane (B) and with the symmetry axis parallel to the image plane (C). Note that the 3D curves of the interpretation of (A) are much more complex than the 2D curves in (A). It is complex because multiple segments of the 3D curves in (B, C) are projected to single segments of the 2D curves in (A). See Demo 2 in the supplemental material for an interactive illustration of the 3D symmetric curves (the demo is also available at: <http://tadamasawada.com/demos/rotsym/>).

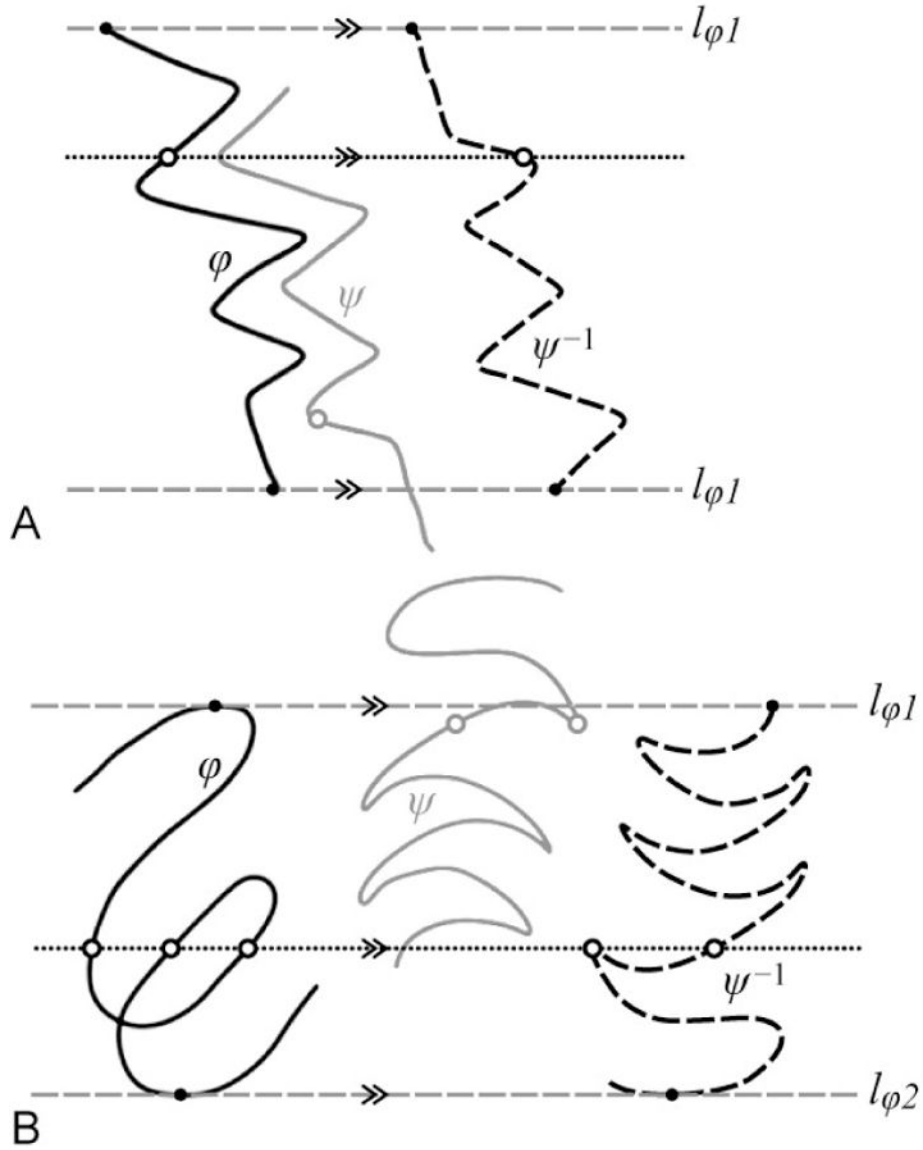


**Figure 13.** Visual method of establishing the correspondence between a pair of 2D curves for its 3D symmetrical interpretation. The pair of the 2D curves  $\phi$  (black, solid) and  $\psi$  (grey solid) (A) in Figure 11A and (B) in Figure 12A and the 180° rotation of  $\psi$  ( $\psi^{-1}$ , black dashed). The curve  $\psi^{-1}$  is translated along  $l_{\phi 1}$  and  $l_{\phi 2}$  for the clarity of the images. The correspondence between  $\phi$  and  $\psi^{-1}$  can be established between intersections (black open circles) of  $\phi$  and  $\psi^{-1}$  with a line (dotted) parallel to  $l_{\phi 1}$  and  $l_{\phi 2}$ . In (A), the parallel line that intersects with  $\phi$  has a unique intersection with  $\psi^{-1}$  and *vice versa*. In (B), the parallel line that intersects with  $\phi$  has one or a finite number of intersections with  $\psi^{-1}$  and *vice versa*. The corresponding points on  $\psi$  are also indicated by grey open circles.

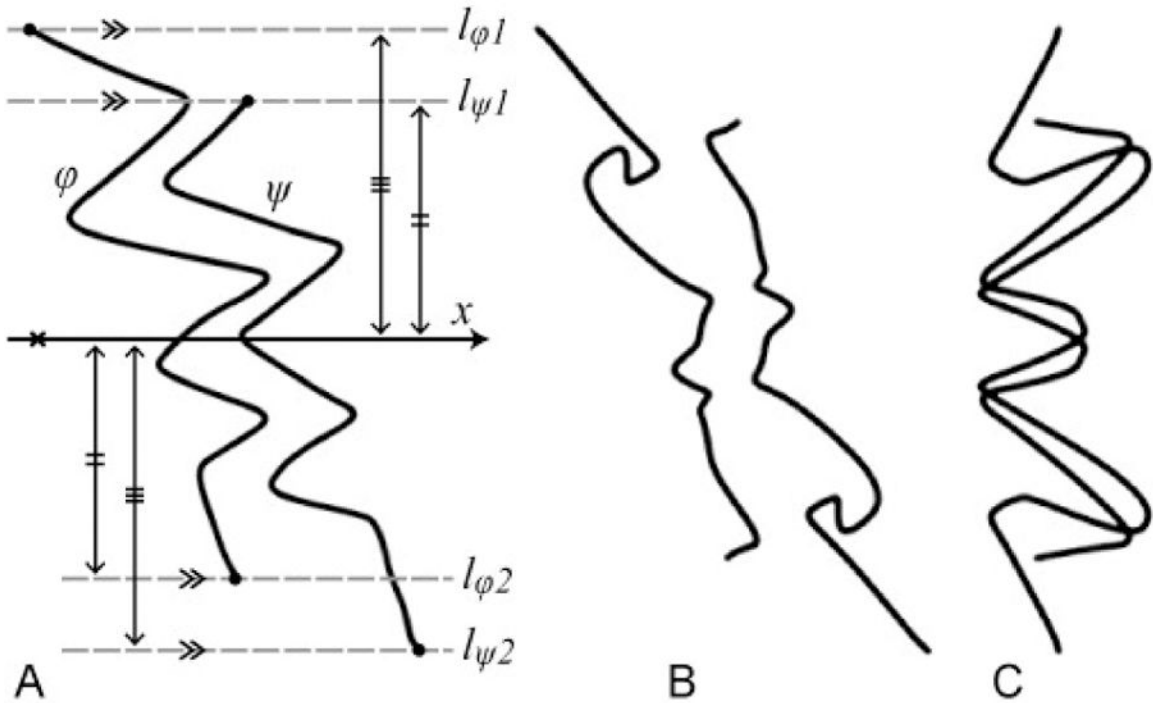


**Figure 14.**

(A) A pair of 2D curves  $\phi$  and  $\psi$  satisfying conditions of Lemma-for-Theorem-A2 and (B, C) two views of their 3D symmetrical interpretation. The symmetrical interpretation was constructed under a perspective projection and its symmetry axis is normal to the image plane. Note that the contours in (A) are identical with those in Figure 11A to allow a comparison between the 3D symmetrical interpretations under the perspective (B, C) and the orthographic (Figure 11B, C) projections. The Principal points of the perspective projection are indicated by 'x'. (B, C) Two orthographic images of the interpretation with its symmetry axis normal to the image plane (B) and with the symmetry axis parallel to the image plane (C). The orthographic projection is used in (B, C) to show the properties of 3D rotational-symmetry under a 2D orthographic projection (Figure 11): the image in (B) is 2D rotational-symmetrical and the image in (C) is 2D mirror-symmetrical. See Demos 3 and 4 in the supplemental material for an interactive illustration of the 3D symmetric curves (the demos are also available at: <http://tadamasaawada.com/demos/rotsym/>).

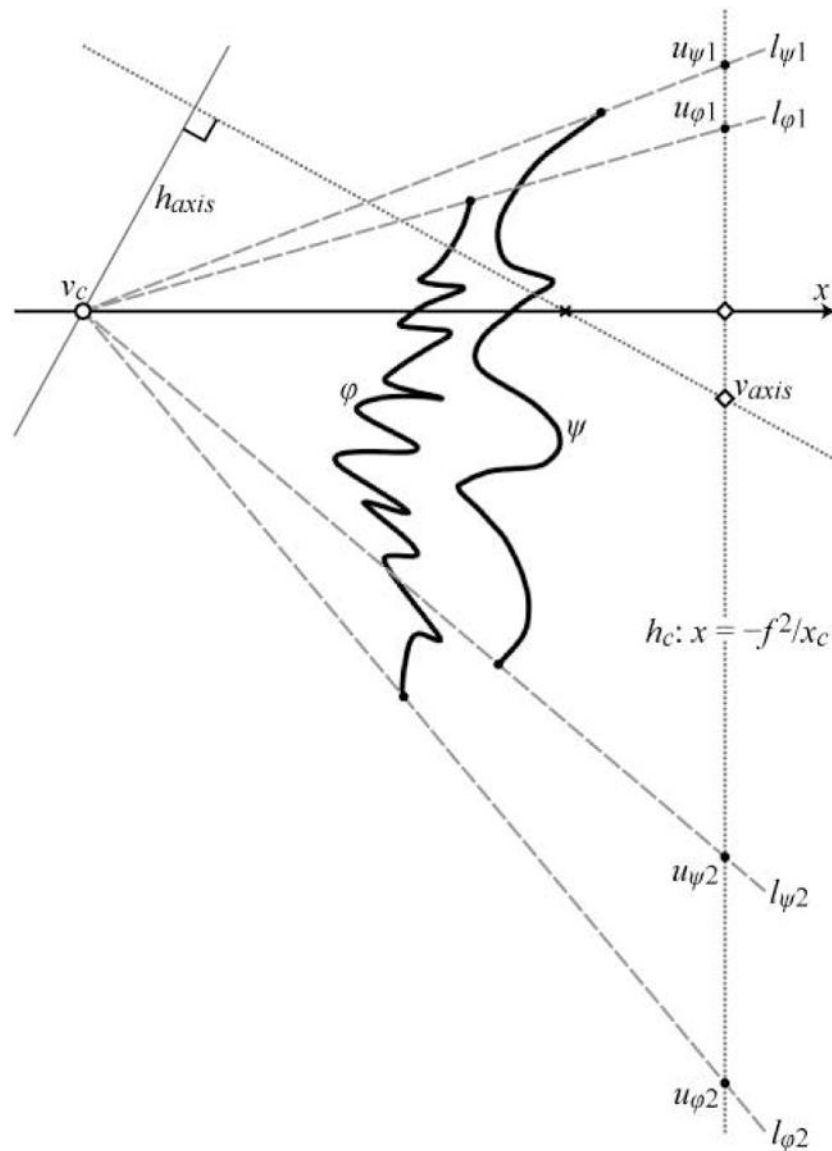


**Figure 15.**

A pair of 2D curves  $\varphi$  and  $\psi$  satisfying conditions of Theorem-A2. The symmetrical interpretation was constructed under a perspective projection (see Demo 5 in the supplemental material for an interactive illustration of the 3D symmetric curves, the demo is also available at: <http://tadamasawada.com/demos/rotsym/>). The Principal points of the perspective projection are indicated by 'x'. The symmetry axis of the 3D interpretation is oriented so that its vanishing point appears at  $v_{axis}$ . The visual angles from  $v_{axis}$  to  $u_{\varphi 1}$  and to  $u_{\psi 2}$  are equal to one another and those from  $v_{axis}$  to  $u_{\psi 1}$  and to  $u_{\varphi 2}$  are also equal to one another.

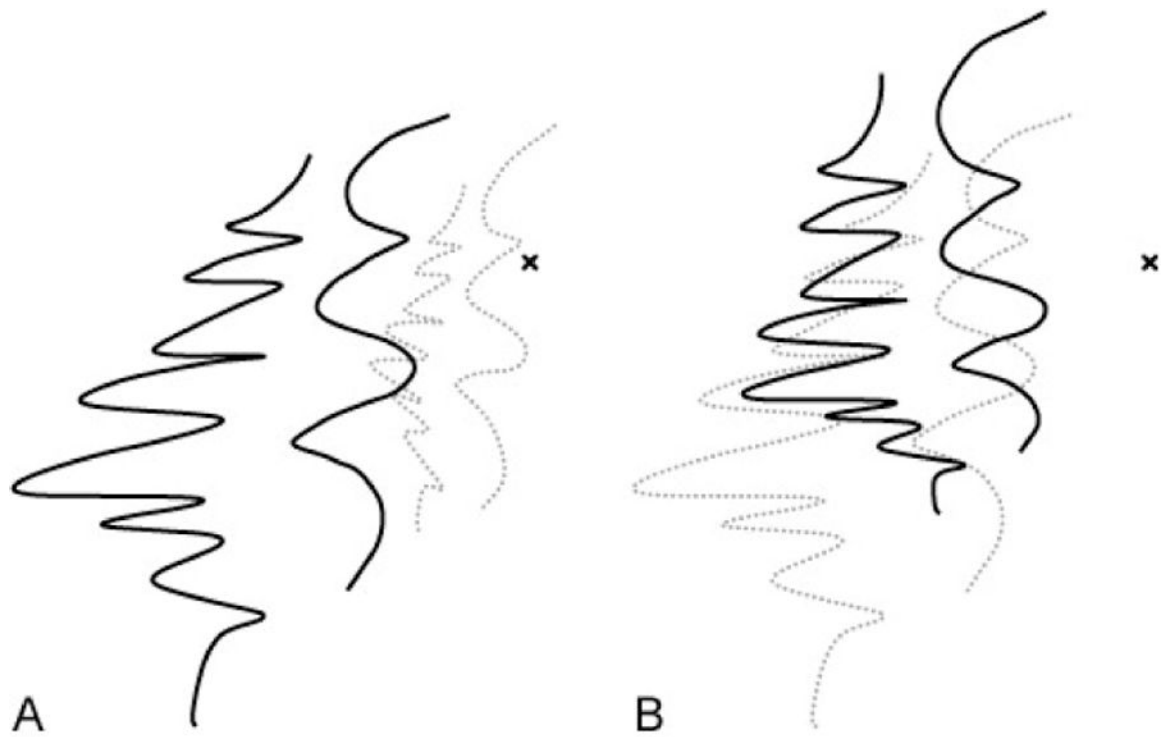


**Figure 16.**

The transformations of the image in Figure 15 after the camera has rotated (A)  $R_{cY}$  and (B)  $R_{cY}R_{cX}$ . (A) The transformed image after  $R_{cY}$  (solid-black) is superimposed to the original image (dotted-grey). (B) The transformed image after  $R_{cY}R_{cX}$  (solid-black) is superimposed to the transformed image after  $R_{cY}$  (dotted-grey). The Principal points of the perspective projection are indicated by 'x'.

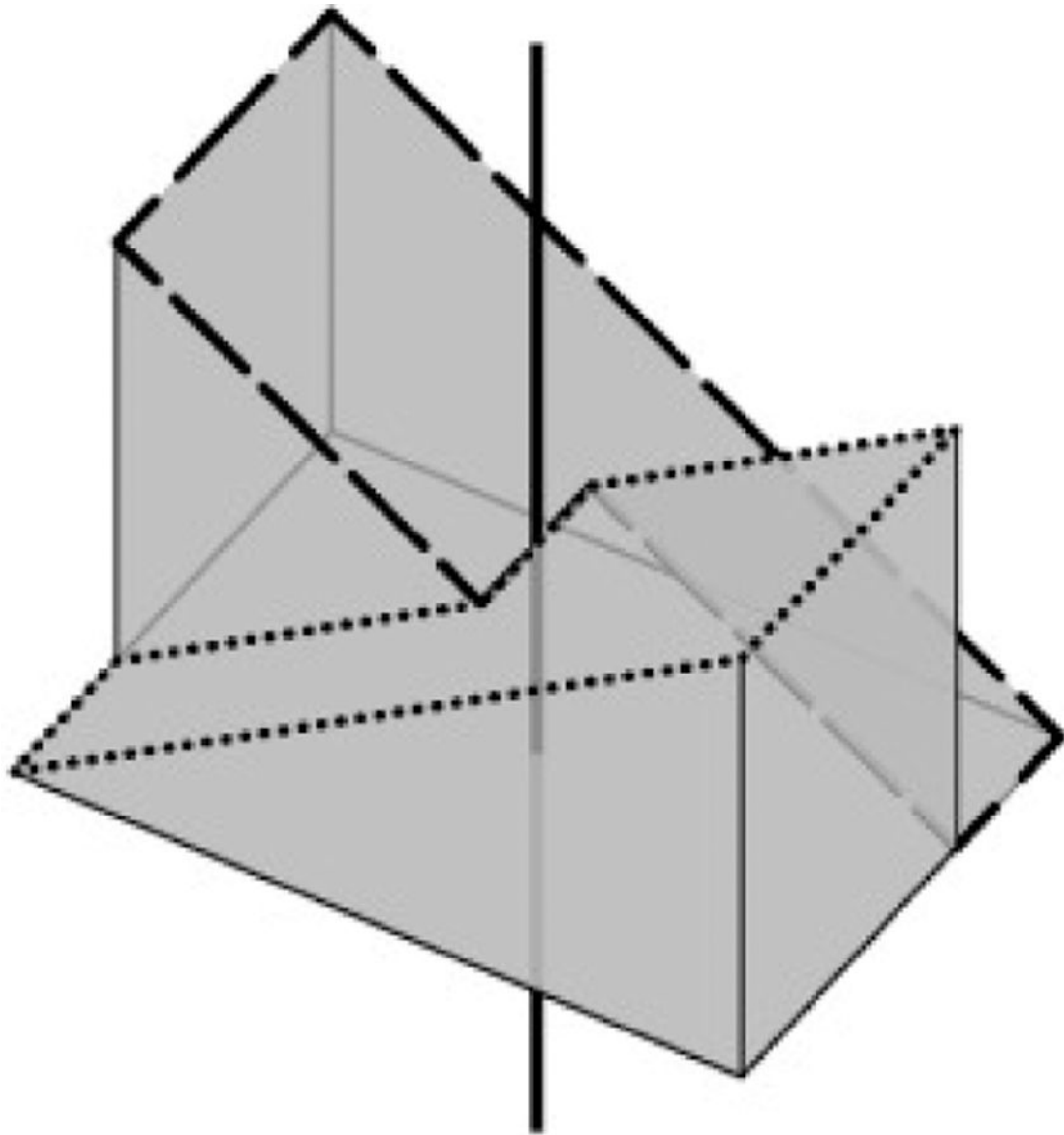


**Figure 17.** An orthographic projection of a rotational-symmetrical object composed of a pair of wedges. Dotted and dashed contours are projections of a symmetrical pair of planar contours of the object. The relationship between their orthographic projections can be represented as a subgroup of the 2D affine transformation (Theorem-B1).

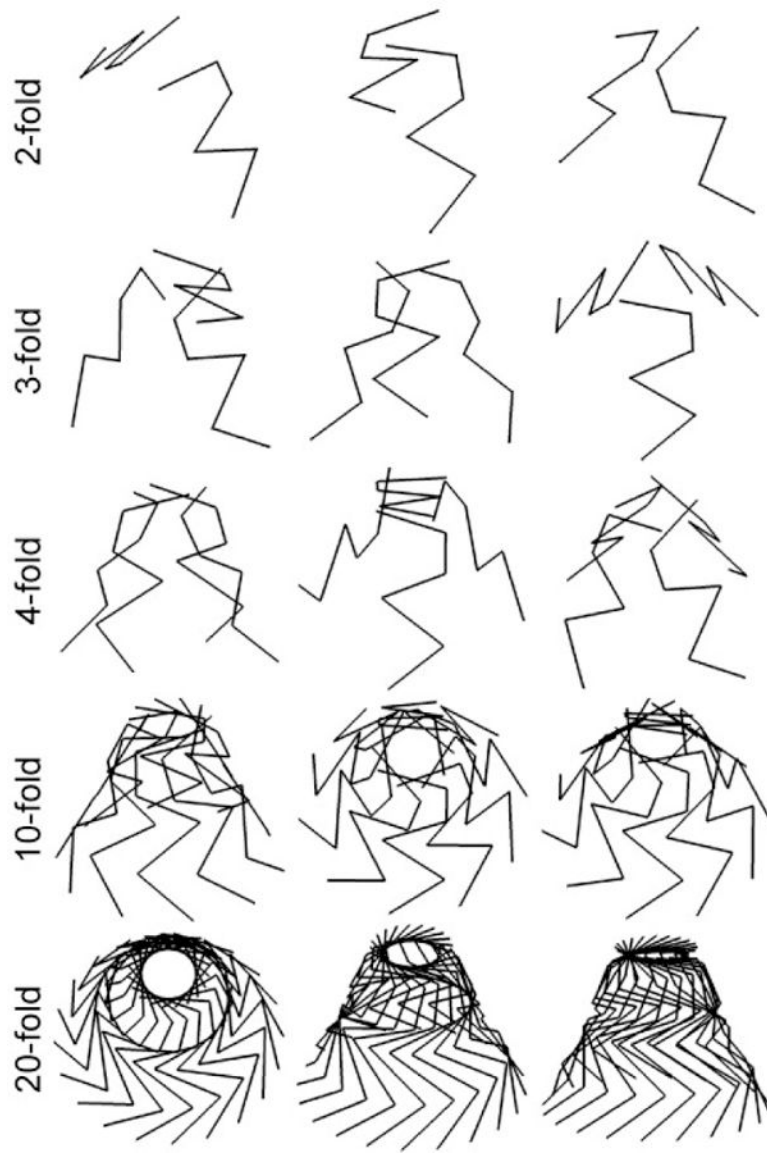


**Figure 18.** Objects composed of planar contours with 2-, 3-, 4-, 10-, and 20-fold symmetry. Three orthographic views of the individual objects are shown in rows.



**Figure 19.** Orthographic views of a surface of revolution from three different viewpoints. The image of the surface of revolution is always mirror-symmetrical under the orthographic projection.

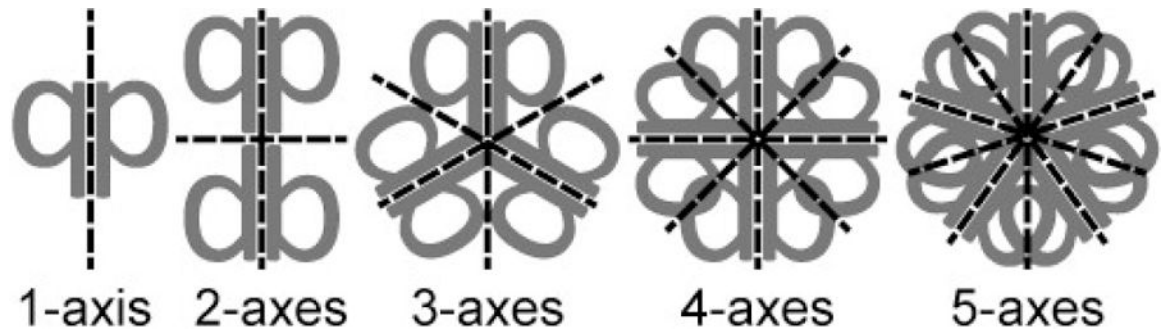


**Figure 20.**

Figures with 1-, 2-, 3-, 4-, and 5-axes of 2D mirror-symmetry. The mirror-symmetrical figures are also 2D rotational-symmetrical if the number of the symmetry axes are more than one.